AD-A031 966   AIR FORCE FLIGHT DYNAMICS LAB WRIGHT-PATTERSON AFB OHIO   F/G 1/3
              LABORATORY TEST AND EVALUATION OF A GRAPHITE EPOXY AIRCRAFT WHE--ETC(U)
              JUN 76   G C SHUMAKER

UNCLASSIFIED   AFFDL-TR-76-54   NL

MICROCOPY RESOLUTION TEST CHART

NATIONAL BUREAU OF STANDARDS-1963

AFFDL-TR-76-54

LABORATORY TEST AND EVALUATION OF A GRAPHITE EPOXY AIRCRAFT WHEEL

MECHANICAL BRANCH
VEHICLE EQUIPMENT DIVISION

JUNE 1976

TECHNICAL REPORT AFFDL-TR-76-54
FINAL REPORT FOR PERIOD JULY 1972 - JULY 1975

D D C
RECEIVED
NOV 15 1976
B

AIR FORCE FLIGHT DYNAMICS LABORATORY
AIR FORCE WRIGHT AERONAUTICAL LABORATORIES
AIR FORCE SYSTEMS COMMAND
WRIGHT-PATTERSON AIR FORCE BASE, OHIO 45433

This report has been reviewed by the Information Office (OI) and is releasable to the National Technical Information Service (NTIS). At NTIS, it will be available to the general public, including foreign nations.

This technical report has been reviewed and is approved for publication.

GERALD C. SHUMAKER
Project Engineer

FOR THE COMMANDER

H.K. BREWER
Acting Branch Chief
Mechanical Branch

ACCESSION for		
NTIS	White Section	☑
DDC	Buff Section	☐
UNANNOUNCED		☐
JUSTIFICATION		
BY		
DISTRIBUTION/AVAILABILITY CODES		
Dist.	AVAIL. and/or SPECIAL	
A		

REPORT DOCUMENTATION PAGE	READ INSTRUCTIONS BEFORE COMPLETING FORM

1. REPORT NUMBER	2. GOVT ACCESSION NO	3. RECIPIENT'S CATALOG NUMBER
AFFDL-TR-76-54		

4. TITLE (and Subtitle)	5. TYPE OF REPORT & PERIOD COVERED
Laboratory Test and Evaluation of a Graphite Epoxy Aircraft Wheel	Final Report. July 1972 — July 1975.
	6. PERFORMING ORG. REPORT NUMBER

7. AUTHOR(s)	8. CONTRACT OR GRANT NUMBER(s)
Gerald C. Shumaker	

9. PERFORMING ORGANIZATION NAME AND ADDRESS	10. PROGRAM ELEMENT, PROJECT, TASK AREA & WORK UNIT NUMBERS
Mechanical Branch (FEM) Air Force Flight Dynamics Laboratory Wright-Patterson Air Force Base, Ohio 45433	Project No. 1369 Task No. 136903

11. CONTROLLING OFFICE NAME AND ADDRESS	12. REPORT DATE
Air Force Flight Dynamics Laboratory Wright-Patterson Air Force Base, Ohio 45433	June 1976
	13. NUMBER OF PAGES
	177

14. MONITORING AGENCY NAME & ADDRESS(if different from Controlling Office)	15. SECURITY CLASS. (of this report)
177 p.	Unclassified
	15a. DECLASSIFICATION DOWNGRADING SCHEDULE

16. DISTRIBUTION STATEMENT (of this Report)

Approved for public release; distribution unlimited.

1369   03

17. DISTRIBUTION STATEMENT (of the abstract entered in Block 20, if different from Report)

18. SUPPLEMENTARY NOTES

19. KEY WORDS (Continue on reverse side if necessary and identify by block number)

Landing gear
Aircraft wheel
Advanced composite
Graphite epoxy material

Structural integrity tests

20. ABSTRACT (Continue on reverse side if necessary and identify by block number)

This report is a detailed description of the laboratory testing of a graphite epoxy aircraft wheel that was designed to fit a Type III, 7.00-8 aircraft tire and withstand the unbraked loads imposed on the A-37B aircraft main wheel. The tests conducted range from the initial pressurization tests to long duration dynamometer slow roll tests. The wheel performed extremely well in these tests and achieved a total of 5,165 roll miles before it developed fatigue cracks. This is more than three times the number of miles required by the MIL-SPEC.

DD FORM 1473   EDITION OF 1 NOV 65 IS OBSOLETE   UNCLASSIFIED
1 JAN 73

012070

qualification requirements for the comparable metal wheel. Since this wheel is the first of its kind and only one wheel was tested, several pictures were taken to closely document the appearance of the composite structure throughout the test. The wheel was instrumented with several strain gages and data were taken for various conditions.

The strains measured are converted to stresses for a two dimensional orthotropic material. These stresses are then compared to the interaction curves developed using composite lamination theory and the maximum allowable strain criteria.

This report is written for a reader who may not be completely familiar with the theory used to characterize composite material structures.

FOREWORD

This report was prepared by Gerald C. Shumaker of the Mechanical Branch (FEM), Vehicle Equipment Division, Air Force Flight Dynamics Laboratory. The work was conducted in-house under Project Number 1369, "Landing Gear Development", Task Number 136903, entitled "Advanced Composite Landing Gear Hardware Development."

The author wishes to express his appreciation to personnel of Systems Research Laboratory, Dayton, Ohio, who instrumented the wheel and conducted the dynamometer tests. These are: Paul C. Ulrich, John Leiter, Bill Humphries and Bill Maggard. Also a special thanks to Oral McCown, who repaired the test wheel several times during its long life.

This report covers research conducted from July 1972 to July 1975.

The report was submitted by the author in March 1976.

TABLE OF CONTENTS

TABLE OF CONTENTS (CONT'D)

LIST OF ILLUSTRATIONS

LIST OF ILLUSTRATIONS (Contd)

LIST OF ILLUSTRATIONS (Contd)

LIST OF ILLUSTRATIONS (Contd)

LIST OF ILLUSTRATIONS (Contd)

LIST OF ILLUSTRATIONS (Contd)

LIST OF ILLUSTRATIONS (Contd)

LIST OF TABLES

LIST OF SYMBOLS

SYMBOL		UNIT
A_{ij}	CONSTANTS USED IN LAMINATE CONSTITUTIVE RELATIONS	psi
E_i	MODULUS OF ELASTICITY	psi
G	SHEAR MODULUS OF ELASTICITY	psi
Q_{ij}	CONSTANTS USED IN LAMINA CONSTITUTIVE RELATIONS	psi
R	ROSETTE STRAIN GAGE	—
S	SINGLE LEG STRAIN GAGE	—
ε_i	NORMAL STRAINS	in/in
γ_{ij}	SHEAR STRAIN	in/in
ν_{ij}	POISSON'S RATIO	—
σ_i	NORMAL STRESS	psi
σ_{ij}	SHEAR STRESS	psi
τ_{ij}	SHEAR STRESS	psi

SECTION I

INTRODUCTION

1. STATEMENT OF THE PROBLEM

The purpose of this work was to experimentally evaluate the
structural integrity of graphite epoxy composite used to construct an
A-37B aircraft main landing gear wheel. One wheel was designed to the
load requirements found in AF Dwg 67J1951 (Reference 1) - A-37B aircraft
(14,000 lb Gross Weight), dated 13 Feb 67 and fabricated by Whittaker
Corporation, Research and Development Division, San Diego, California.
(Reference 2). The test article was constructed from meter-length and
mid-length Modmor II fiber which had been preimpregnated (prepreg) with
Union Carbide 4617 epoxy resin. The braking requirements for the wheel
were not considered, consequently no slots were cut or formed in the
brake-half of the wheel. One graphite epoxy wheel was procured for test.
The fabrication details of this wheel are contained in Reference 2.
All testing was done in the Air Force Flight Dynamics Laboratory's
Landing Gear Test Facility at Wright-Patterson Air Force Base, Ohio.

2. INTENT OF TESTING

Simply stated, the intent of the testing was to learn as much as
possible about the structural characteristics of one 7.00-8 graphite
epoxy aircraft wheel. The wheel was tested according to the corresponding
metallic wheel qualification requirements found on AF Dwg 67J1951
(Reference 1). At the outset of the tests, the assumption was made that
the wheel could fail prematurely and thus caution prevailed. Accordingly,

1

the tests were pursued carefully and slowly, especially during the initial
pressurization. Strain data were collected for pressurization, static
load, and radial and camber rolling load. Roll tests were conducted
until the structure could not be rolled any longer. These tests were then
followed by burst pressure testing.

3. SUMMARY OF TEST LOADS

The conditions used to test the graphite epoxy wheel were obtained
from AF Dwg 67J1951. This drawing describes the performance requirements
to be fulfilled in order to qualify a production wheel of this size. No
brake tests were planned for this wheel; therefore, the braking
requirements are not listed. The qualification loads are:

(1) Normal inflation pressure - 120 psi
    Burst test inflation pressure - 406 psi

(2) Straight roll test to be for 1400 miles at 6150 lbs
    radial load.

(3) Combined radial - side load roll test to be for 400 miles
    at 6254 lbs radial load and 1564 lbs side load - acting
    inboard. The inboard side of the wheel is the "Non-brake"
    half.

(4) Combined static limit loads are:

        5,930 lbs side load
        14,830 lbs radial load

(5) Combined static ultimate loads are:

        8,900 lbs side load
        22,250 lbs radial load

SECTION II

DESCRIPTION OF THE TEST WHEEL
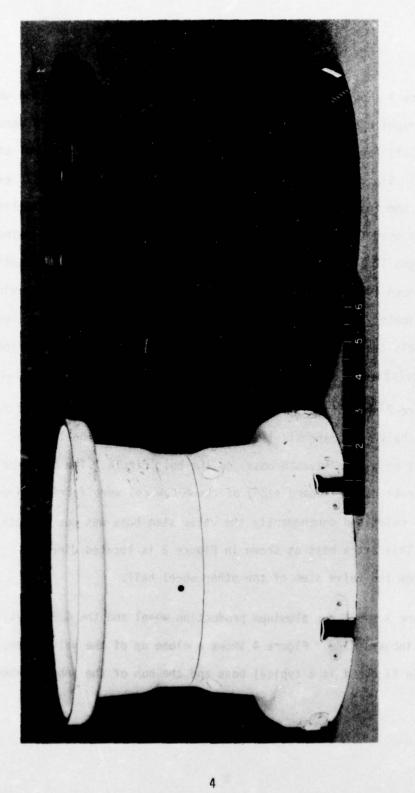
Figure 1 shows the comparison between the aluminum production wheel and the graphite epoxy (G/E) wheel. Notably absent from the G/E wheel are the slots for the brake rotor and the fuse plugs in the barrel of the wheel. Since the primary intent of this program was the basic evaluation of the feasibility of using G/E in this application, a simplified design was used for the initial approach to the problem. The aluminum wheel weighs 12.1 lbs and the G/E wheel weighs 10.1 lbs for the configuration shown in Figures 1 through 3. This amounts to a weight savings of approximately 16%. Naturally, the inclusion of the wheel bearings in these wheels (the same bearing is used in both the aluminum and graphite epoxy wheels) would slightly lower the per cent weight savings attained.

Figure 2 shows the aluminum wheel and the G/E wheel as viewed from the brake-half (outboard side). Noticeable on the G/E wheel is an additional boss (the seventh boss) on the bolt circle. The brake-half and the non-brake-half (inboard side) of the G/E wheel were fabricated on identical molds and consequently the valve stem boss was put on both halves. This extra boss as shown in Figure 2 is located directly across from the valve stem of the other wheel half.

Figure 3 shows the aluminum production wheel and the G/E wheel viewed from the inboard side. Figure 4 shows a close up of the valve stem. Also visible in Figure 4 is a typical boss and the hub of the inboard wheel half.

Figure 1. AL Production Wheel and Graphite Epoxy Test Wheel
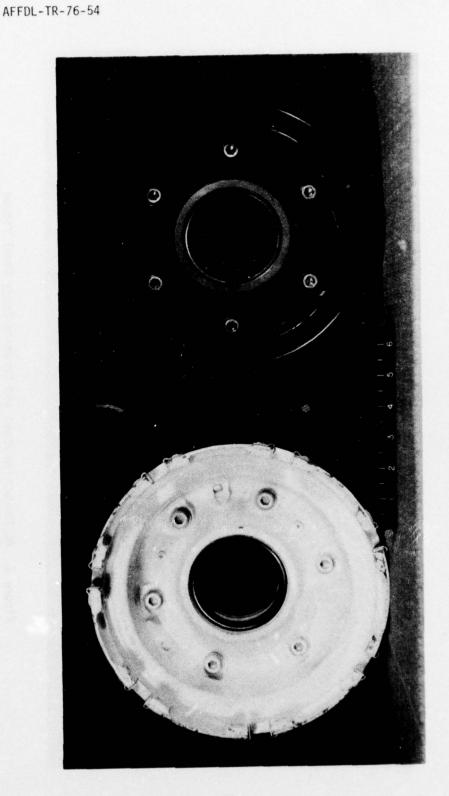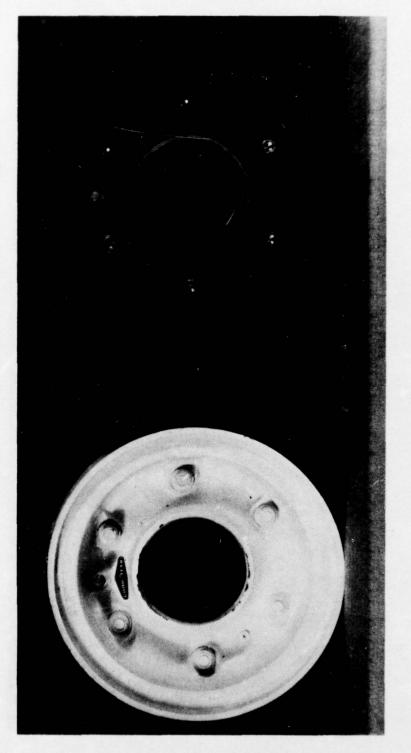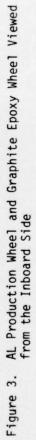
Figure 2. AL Production Wheel and Graphite Epoxy Wheel Viewed from the Brake (outboard) Side

Figure 3. AL Production Wheel and Graphite Epoxy Wheel Viewed from the Inboard Side

Figure 4. Valve Stem (on inboard side)
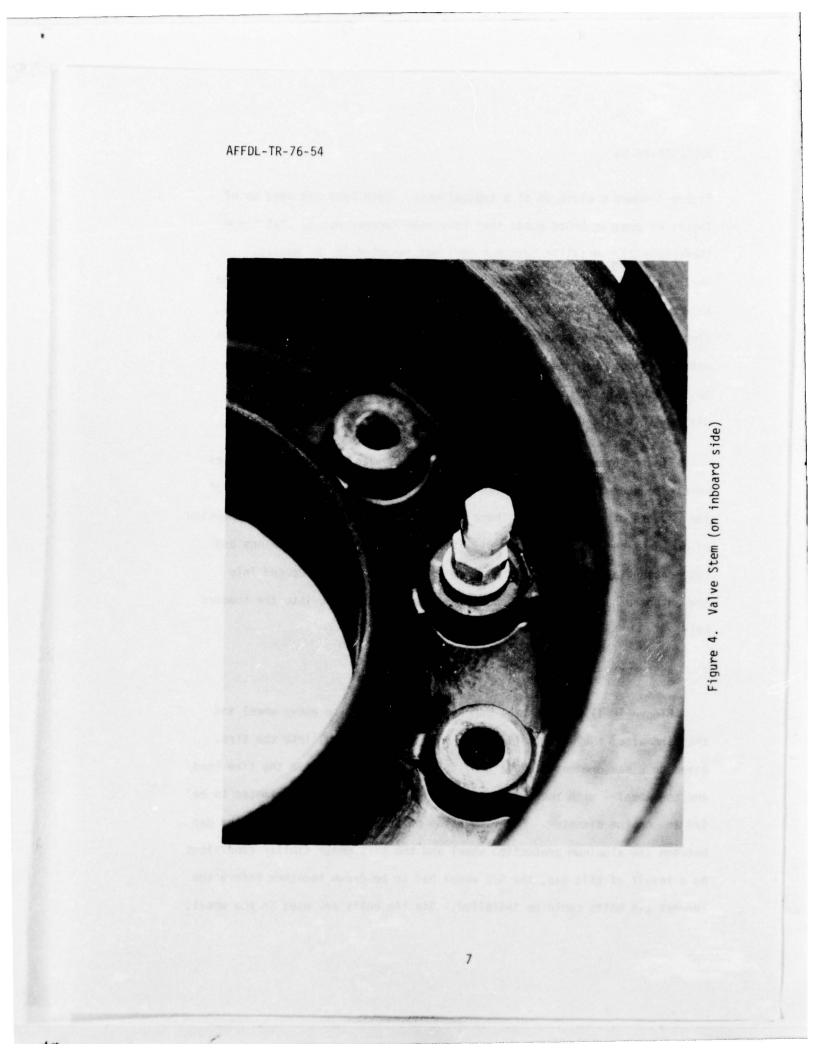
Figure 5 shows a close up of a typical boss. Each boss was made up of layers of prepreg broad goods that have been punched out to that shape (Reference 2). Metallic bushings were not inserted in the bosses. The holes were drilled through (in two operations) from one side of the assembled wheel. When the finish drill protruded from the bottom side (inboard side), two bosses broke off (delaminated) from the base of the outboard side. Repair was achieved by bonding the separated boss back to the hub with room temperature cured epoxy and clamping the boss in place with a bolt until the epoxy cured (Reference 2).
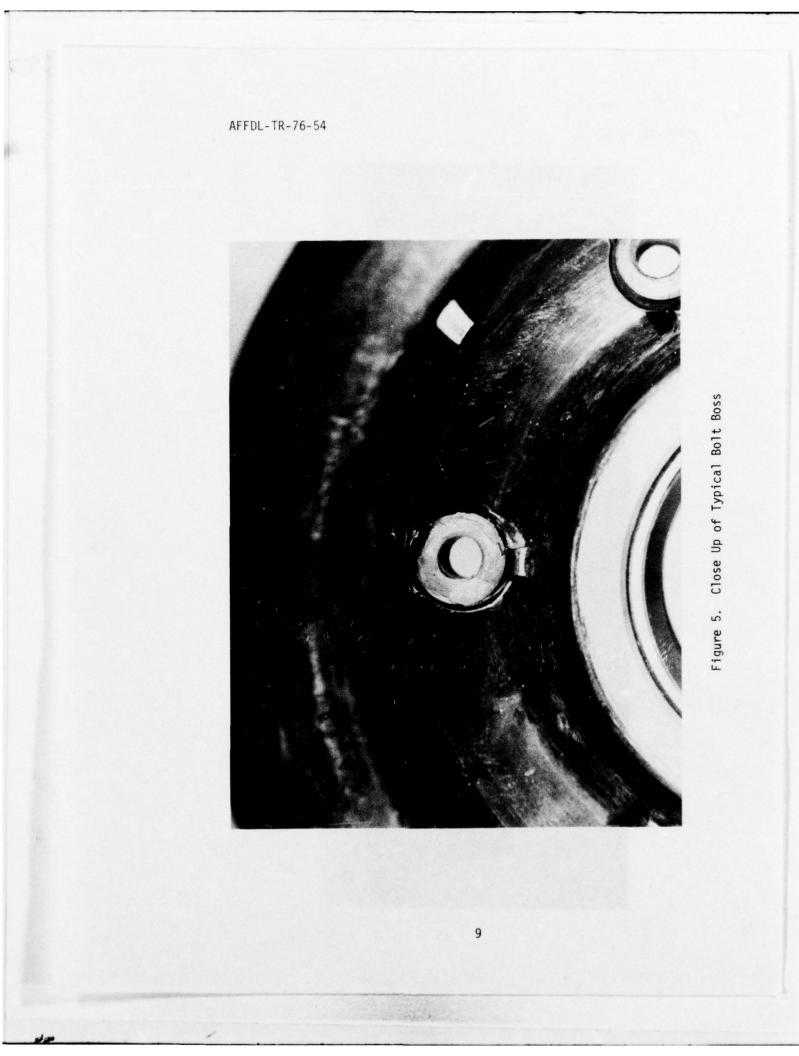
Figures 6 and 7 show the disassembled G/E wheel. Some difficulties were encountered in machining the "O" ring groove due to delamination of the corners of this groove. These defects were repaired with the exception of one area as shown in Figure 8. Figure 9 presents the dimensions and fabrication layup of the test wheel. An aluminum hub was bonded into the outboard half with epoxy adhesive and was a slip fit into the inboard half.

1. ASSEMBLY OF THE TEST WHEEL

Figure 10 illustrates the gap between the graphite epoxy wheel and the tire after the wheel half had been pressed (by hand) into the tire. Based on a measurement of this gap, the interference between the tire bead and the wheel - with the tire seated against the rim - was estimated to be 1/8 in. on the diameter. For comparison purposes, Figure 11 shows the gap between the aluminum production wheel and the tire under similar conditions. As a result of this gap, the G/E wheel had to be drawn together before the correct tie bolts could be installed. Six tie bolts are used on the wheel,

Figure 5. Close Up of Typical Bolt Boss

Figure 6. Side View - Disassembled Graphite Epoxy Wheel

Figure 7. Disassembled Graphite Epoxy Wheel

Figure 8. Close Up of "O" Ring Groove Showing Delamination

.03 MACHINING ALLOWANCE

.05 MACHINING ALLOWANCE

.03 MACHINING ALLOWANCE

.05 MACHINING

BOSS - (7) PLACES
LOCATE ON 6.25 DIA CIRCLE
(6) EQUALLY SPACED PLUS
(1) CENTERED BETWEEN
TWO BOSSES AS SHOWN

.80 DIA
CENTERED ON
6.25 DIA CIRCLE

1.06 (7) PLACES

3 THESE SURFACES TO BE
AS MOLDED. DO NOT
MACHINE

.396/.390 DIA
(7) HOLES EQUALLY
SPACED ON 6.250
DIA CIRCLE

.12 ± .06 R
(TYP)

**TYPICAL CROSS SECTION
OF BOSS - (7) PLACES**

-1 DETAIL

LAY-UP SCHEDULE

NOMINAL FIBER THICKNESS: .007 INCH/PLY

LAYER #	A	B	C	D	E	F	G	H	I	J	K
1			6 CIRC			3 CIRC	6 CIRC				
2			3 R/A			2 R/A	4 R/A				
3			2 CIRC			3 CIRC	4 CIRC				
4			3 R/A			2 R/A	4 R/A				
5			4 ± 45°			2 ± 45°	4 ± 45°				
6			4 CIRC			3 CIRC	4 CIRC				
7			2 R/A			1 R/A	4 R/A				
8			4 ± 45°			4 ± 45°	4 ± 45°				
9			2 CIRC			3 CIRC	4 CIRC				
10			2 R/A			1 R/A	4 R/A				
11			4 ± 45°			2 ± 45°	4 ± 45°				
12			2 CIRC			3 CIRC	4 CIRC				
13	3 R/A		2 R/A				4 R/A				
14	5 CIRC		5 CIRC				4 CIRC				
15								2 R/A			
16								2 ± 45°			
17								2 CIRC			
18								1 R/A			
19								2 ± 45°			
20								4 CIRC			
21									4 R/A		
22									4 CIRC		
23									4 R/A		
24									4 CIRC		
ETC. REQD									ETC.		

STATION

TAPER
SEE SKETCH

LEGEND:
CIRC - CIRCUMFERENTIAL FIBER
R/A - RADIAL/AXIAL FIBER
± 45° - FIBER ORIENTATION ± 45° TO AXIS OF ROTATION
- NUMBER OF PLIES

STATION
LAYER

LAYER # 5

LAYERS 1, 2, 3, ETC
AS REQUIRED

Figure 9. Drawing of the G/E Test Wheel

13

SECTION A-A

3.75

NOTES: UNLESS OTHERWISE SPECIFIED:
1. DO NOT SCALE DRAWING. WORK TO DIMENSIONS GIVEN
2. DRAWING INTERPRETATION PER MIL-D-1000
3. MACHINED FILLET RADII .03. BREAK ALL SHARP
   CORNERS .015-.005 R
4. ANODIZE -4 & -5 ALL OVER PER MIL-A-8625, TYPE I
5. THESE DIMENSIONS ARE SAME AS FOR THE EXISTING
   METAL MOLD. ALL OTHER DIMENSIONS HAVE BEEN
   CHANGED
6. APPLY EA 934 EPOXY ADHESIVE (DEXTER HYSOL) OR
   EQUIV. TO -5 AND HAS NOT DOWEL PIN PRIOR TO
   INSTALLING IN -3.

MS 20006-34 BOLT - (6) REQD
MS 21042-6 NUT - (6) REQD
MS 20002 C6 WASHER-INSTALL
WITH C'SINK SIDE TOWARDS
BOLTHEAD — (12) REQD

4 SEE DETAIL.

SEE DETAIL
.562 ± .005 DIA HOLE THRU
C'BORE PER SIDE .625 DIA × .010 DEEP
(-3 ONLY)
5766 VALVE (SCHRADER)
MS 29512-2 O-RING

WHEEL ASSEMBLY - GRAPHITE
COMPOSITE

Whittaker

SIZE: C | CODE IDENT NO. 83472 | DRAWING NO. 4618

SHEET 1 OF 10

Figure 10. Gap Remaining with Tire on G/E Wheel (Tie Bolts Not Installed)

Figure 11. Gap Remaining on Aluminum Wheel Under Same Conditions

15

and so to draw the wheel together, longer bolts were placed in three equally spaced holes and tightened until three of the proper wheel bolts could be installed.

Figure 12 shows the "O" ring placed in the "O" ring groove. The "O" ring is not retained in the "O" ring groove, thus assembly of the wheel halves must be done with the wheel in the horizontal position. However during the drawing operation described above, the wheel was occasionally titled and this resulted in a pinching of the "O" ring. When this occurred, the wheel would not retain air and had to be disassembled and a new "O" ring installed.

Once the wheel bolts were fully torqued (15 ft-lb), a gap remained between the wheel and the tire as shown in Figure 13. At approximately 20 psi, the tire seated against the outer flange. Prior to assembly, a liberal coating of silicon grease was spread on the barrel of the wheel and the aluminum hub. This was done to reduce the tendency for the tire to cling to the wheel during disassembly.

During the very first assembly of the wheel, an attempt was made to torque the tie bolts to 17 ft-lb as recommended by the contractor. However, as the torque level approached 17 ft-lb a crunching sound was heard. The graphite epoxy lugs were apparently being crushed at a torque greater than 15 ft-lb. Thus, to prevent further crushing, the tie bolt torque was reduced to 15 ft-lb for all subsequent assembly operations.

Figure 12. "O" Ring Placed in Groove
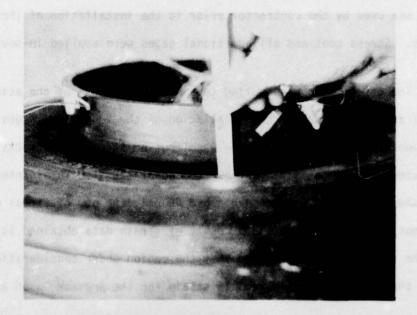
Figure 13. Gap Remaining After Wheel Halves Were Bolted Together

17

2. STRAIN GAGE LOCATIONS

Figures 14 and 15 depict the strain gage locations on the wheel halves. Gages R_1 through R_{10} are rosette gages with 120 ohm resistance and 1/4 in. gage length.   Gages R_{11}, R_{12}, and R_{13} are rosette gages with 120 ohm resistance and 1/16 in. gage length.

Later on in the rolling tests, the bead seat rosette gages (R_{12} and R_{13}) were damaged due to the relative motion between the tire and the wheel. These gages were replaced with identical gages numbered R_{14} and R_{15}.

All the single gages, S_1 through S_{12} and three temperature compensating gages have 120 ohm resistance and 1/16 gage length.

Gages R_1 through R_9 were installed by the contractor. No stress coat was used by the contractor prior to the installation of these gages. Stress coat and all additional gages were applied in-house.

The stress coat was applied to a quarter segment of the assembled wheel and tire prior to the installation of the additional gages. A maximum of 40 psi was put in the wheel but no stress coat cracks were detected. Since initial doubt existed about the structural integrity of the wheel subjected to pressure above 40 psi, the use of stress coat was not pursued further. As a result of strain data obtained later in the testing, it was learned that the region under consideration had less than 400 micro-in/in tensile strain for the pressure used and this was
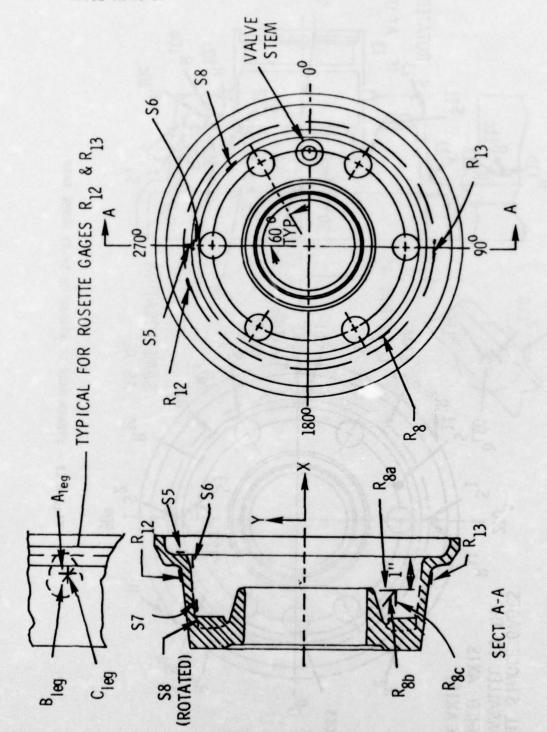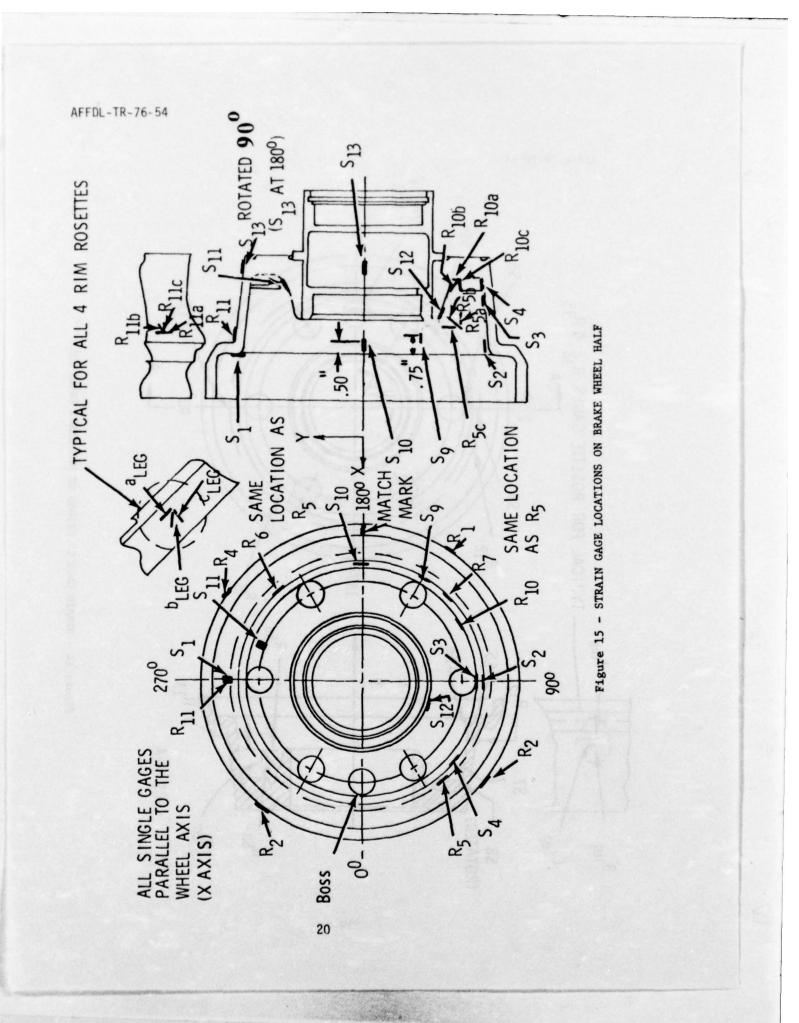
Figure 14 - STRAIN GAGE LOCATIONS ON NON-BRAKE WHEEL HALF

Figure 15 - STRAIN GAGE LOCATIONS ON BRAKE WHEEL HALF

20

below threshold of the stress coat used. Several gages were installed at similar locations where the strain should be approximately the same during pressurization. Gages on which similar readings would be expected are:

1) R_1, R_2, R_3, R_4

2) R_5, R_6, R_7, R_8

3) R_9, R_{10}, (R_9 was defective)

4) R_{11}, R_{12}, R_{13}

5) S_1, S_5

6) S_2, S_6

7) S_3, S_7

8) S_4, S_8

9) S_9, S_{10}

21

SECTION III

TEST EXPERIENCE

The tests applied to the wheel were initially done in an extremely
cautious manner until the wheel had demonstrated its structural integrity.
The graphite composite parts of the wheel withstood the pressurization
loads, the flat plate loads, all the required Air Force specification
straight and camber roll miles and finally an additional 3,756 miles of
straight roll before they failed in fatigue. The wheel did not fail
catastrophically, as might happen with a metal wheel, but instead just
gradually began to lose air. From all aspects, the test of this wheel
demonstrated it to be fully capable of withstanding the non-braked
requirements of the comparable metal wheel.

1. PRESSURIZATION

The wheel was pressurized in 20 psi increments to the rated pressure
of 120 psi with no problems. Large amounts of strain data were taken
during the initial pressurization and attempts were made to determine
if any creep of the composite structure occurred. These data are discussed
in Section IV. The wheel held 130 psi for approximately 72 hours with
less than 10 psi leakage over this time period. There were no audible
noises emitted from the composite during any of the pressurization up to
130 psi. Later, after the required qualification dynamometer slow roll
(1,800 miles total) had been completed, the unloaded wheel was incre-
mentally pressurized up to 250 psi. At approximately 240 psi, the
composite structure emitted the first audible cracking sounds. An
inspection of the wheel revealed three very smal' cracks in the bead seat

22

area. These cracks, however, did not preclude the additional ensuing

dynamometer slow roll tests.
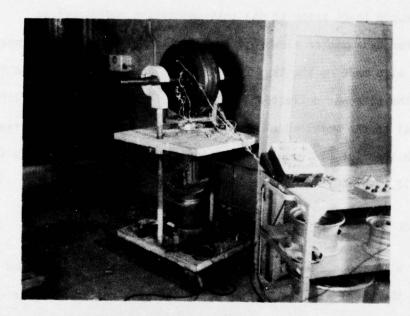
Figure 16. Loading The Wheel On A Flat Plate

2. STATIC LOAD TESTS AND FOOTPRINT MEASUREMENTS

The wheel was first loaded using a flat plate mechanism as shown in

Figure 16. During pressurization the largest strain was found at a bead

seat rosette strain gage. This gage was then centered on the flat plate

directly over the load and closely monitored as the load was increased.

The tire was inflated to the rated pressure of 120 psi and the load was

increased gradually up to the rated radial load of 6150 lbs. Strain

data were taken from the bead seat and other strain gages at 20%

increments of the rated straight roll load. The maximum strain of

2100 micro-in/in (found at the bead seat gage) at rated load was

approximately 30% greater than that attained at 130 psi and this strain

23

level was assumed to be conservative for a composite structure. No audible noises were emitted from the structure during the static loading. The flat plate static tests were done primarily to verify that the wheel would withstand the rated loads prior to the instrumentation modifications necessary for dynamometer slow roll tests. Flat plate deflection measurements were also made on the test rig of Figure 16. These measurements indicated the tire was deflected 35% under the rated load, a condition that is identical to the metal wheel under similar conditions. A footprint of the tire on the flat plate under rated load was also taken and this is shown in Figure 17.

3. INITIAL DYNAMOMETER SLOW ROLL AND DATA COLLECTION
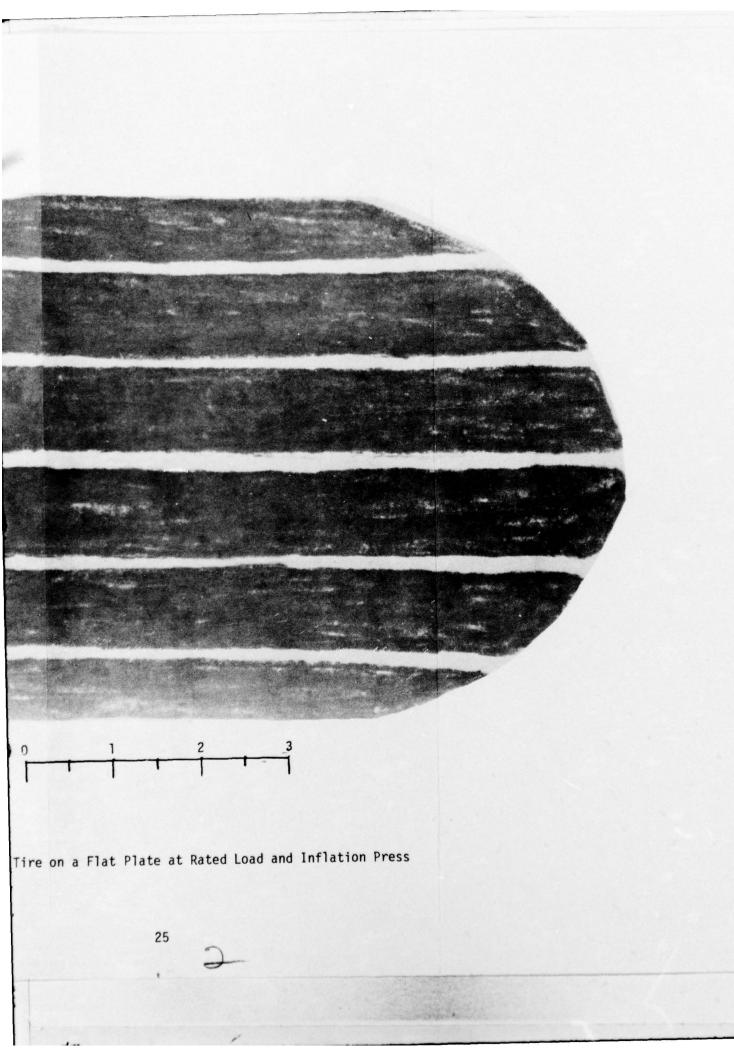
After a thorough analysis of the data from the static tests had been performed, the wheel was then prepared for the slow roll dynamometer tests. As shown in Figure 18 a connector was installed on the wheel and the strain data were transmitted through a long cord attached to the wheel. During the test the dynamometer was brought up to a very slow constant speed with the wheel in the "unlanded" position. The wheel was then "landed" against the dynamometer, allowed to roll three to five revolutions and then "unlanded". The long cord was allowed to twist during the test. Following each run, to untwist the cord, the wheel was manually rotated an equal number of turns in the opposite direction. Data were taken from a total of six rosette gages and eight single gages. There were connector plugs on each side of the wheel, thus to collect all the data it was necessary to reverse the wheel on the mandrel. Since the strain would be plotted vs the angle of rotation, the angular location of each gage with respect to the reference point, 0 at the value stem, was carefully
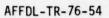
RATED INFLATION .... 120 PSI
.....% RATED LOAD .... 6150 LBS.
    35% DEFLECTION

MAX. FOOTPRINT LGTH...... 9.875 IN.
MAX. FOOTPRINT WDTH...... 5.750 IN.
NET CONTACT AREA .... 42.33 SQ.IN.
GROSS CONTACT AREA...... 48.56 SQ.IN.

SCALE(IN.) 0   1
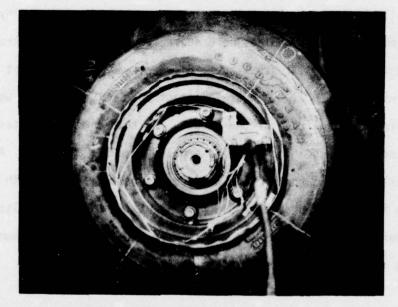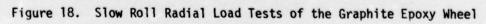
Figure 17.   Footprint of the Tire on a Flat Pla

0   1   2   3

Tire on a Flat Plate at Rated Load and Inflation Press

Figure 18. Slow Roll Radial Load Tests of the Graphite Epoxy Wheel

27
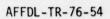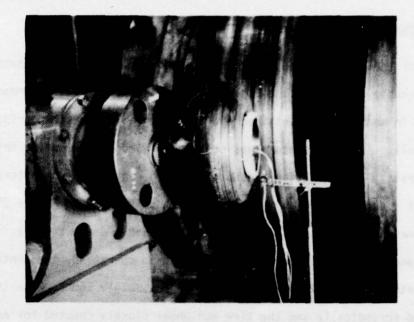
noted for each position of the wheel, as shown in Figure 18 or reversed. Straight slow roll tests were first completed and then the camber slow roll tests were completed. A 15° cambered mandrel was available for use and this most nearly introduce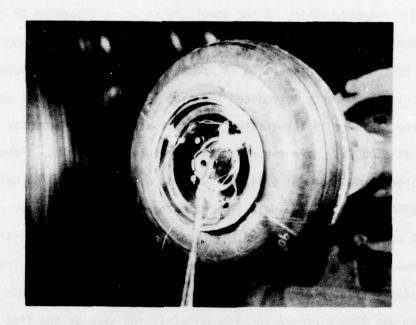d the side load required by the qualification drawing. Figure 19 illustrates this test setup. A dynamometer carriage load of 6100 lbs gave the required side load of 1570 lbs although the required normal load of 6254 lbs was not met (the actual normal load was 5900 lbs). All the data from both the straight and camber slow roll tests were carefully analyzed before any further tests were started. The maximum strain was again found at the same bead seat rosette from which the static (flat plate) data were taken. The magnitude of this maximum strain was 2100 micro-in/in (approximately the same as the flat plate tests) for both the straight and camber slow roll. The rated inflation pressure of 120 psi was used for these tests.

All the initial slow roll tests were completed without any significant problems. No audible noises were heard from the composite structure during the slow roll tests. When the wheel was landed against the flywheel there was always a small impact load but no attempt was made to determine the magnitude of the impact. By this time in the testing, the wheel had been assembled and disassembled a number of times. As pointed out earlier, the barrel of the wheel was liberally coated with silicone grease to aid in the disassembly process. Extreme care was also used in the tear down process (Figure 20) to keep the side loads encountered during disassembly as low as possible.

Figure 19. Slow Camber Load Tests of the Graphite Epoxy Wheel

4.   STRAIGHT SLOW ROLL TESTS

For these tests, the wheel and tire cavity were instrumentated with a thermocouple that was placed through the valve stem. This thermocouple served to measure the contained air temperature in the tire 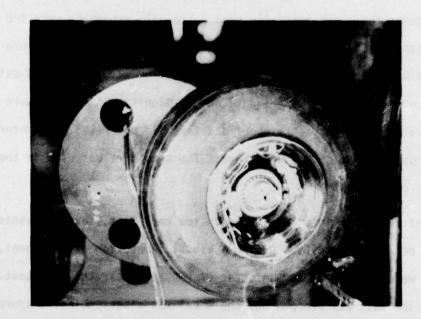during the slow roll. This temperature was continuously monitored during the slow roll tests. The inflation pressure was also continuously monitored and kept at a constant 120 psi. This test setup is shown in Figure 21. The dynamometer speed was held below 6 mph and averaged about 4 mph. At this speed and with the dynamometer cooling fan in operation, the contained air temperature of the tire stabilized at approximately 160°F. The test was stopped periodically and the tire and wheel closely checked for any signs of structural deterioration.

At 140 miles into the straight slow roll test, data were taken from the same gages that were initially read. The only exception were the two bead seat gages. These gages were now inoperative and apparently were destroyed by the motion between the tire bead and the wheel. The strain data taken were compared to the initial data and no significant changes were found. A visual inspection of the wheel and tire did not reveal any deterioration and thus the testing was continued. The same tire was used in the continuation of the tests.

At 260 miles into the straight slow roll test, several events occurred which delayed the tests. During a visual inspection of the wheel, crazing lines were discovered in the outer flange area near the bead seat. At this point the test was stopped and the wheel was disassembled. Figure 22 illustrates the wheel immediately after disassembly. A crack was discovered in the composite structure near the Al hub and this is shown in Figure 23.
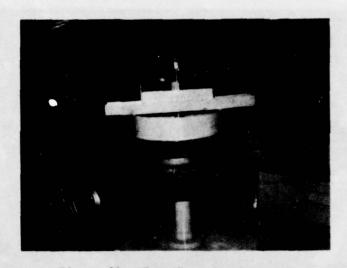
Figure 20. Tear Down Processes
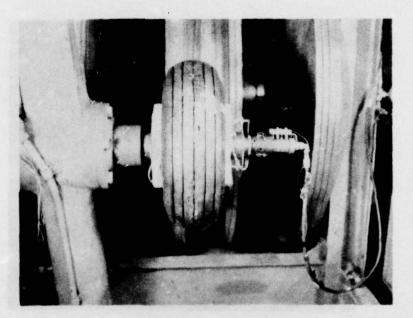
Figure 21. Straight Roll Tests

Figure 22. Disassembled Wheel After 260 Miles of Straight Roll
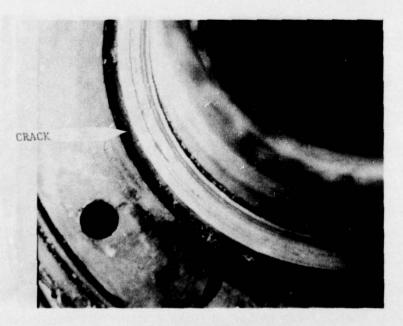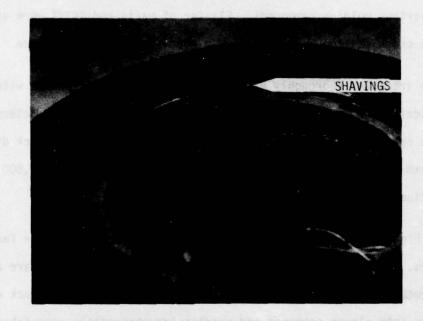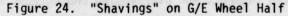
Figure 23. Crack in Composite Near AL Hub

This crack appeared to extend over approximately 120° of the circumference. Figure 23 also shows what appears to be graphite epoxy "chips" or shavings in the cavity near the base of the Al hub. Figure 24 shows the graphite epoxy shavings on the opposite wheel half. This figure also shows what appears to be a wear area on this wheel half. The Al hub (Figure 22) also was showing signs of wear. The explanation for the wear which occurred between the Al hub and the composite structure will be discussed in subsequent paragraphs.

Figure 24. "Shavings" on G/E Wheel Half

At this point all efforts focused on determining the severity of the crack near the Al hub. The hub was firmly attached to the wheel and could not easily be removed, so this naturally hindered the inspection. The nondestructive test (NDT) inspection most readily available was the X-ray process. Low energy X-ray radiation techniques were attempted but the complex shape of the region near the crack precluded its detection.

Various Dye Penetrants were used in an effort to make the crack more visible for photographic purposes. A red, visible, water soluble dye was partially effective in exposing the crack but was difficult (extremely messy) to use. Fluorescent penetrant dyes were also tried but these also were only partially successful in exposing the details of the crack. Black light photographic equipment was not readily available and thus the fluorescent penetrant dyes were not used to their full capability.

Attempts were also made to make a permanent imprint of the crack by using various molding compounds. Plaster of paris and "RTV" were used but the crack was too small to allow a good impression to be made.

The crack was thoroughly examined under a stereo microscope with a magnification up to 50X. The depth of the crack could not be determined but the crack appeared to turn inward toward the hub. This crack did grow into a delamination which will be discussed later in the 1,000 mile inspection.

In Figure 25 a dime and a 0.010 in. wire are shown for scale factor purposes. Based on this photograph, the pictures of the crack are a 4X representation of the actual part. The entire length of the crack was split up into eleven segments and overlapping photographs were taken. These pictures are shown in Figures 25 through 28.

Figure 29 shows a typical bolt boss at 260 miles. Although small fragments of the composite broke away from the boss no severe delaminations of any of the bosses were detected during any of the roll tests. Figure 30 shows what appears to be crazing lines near
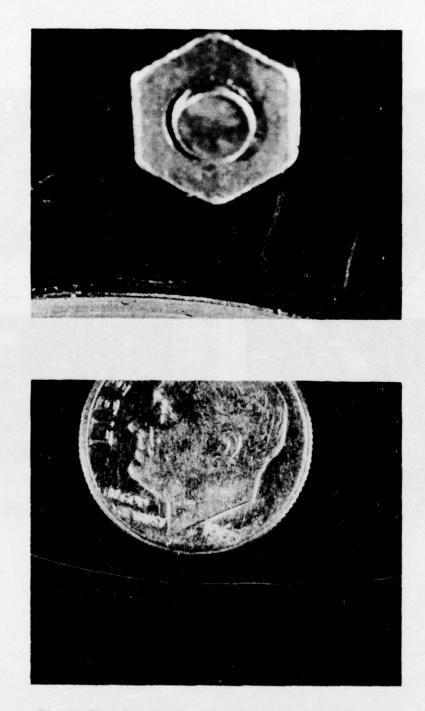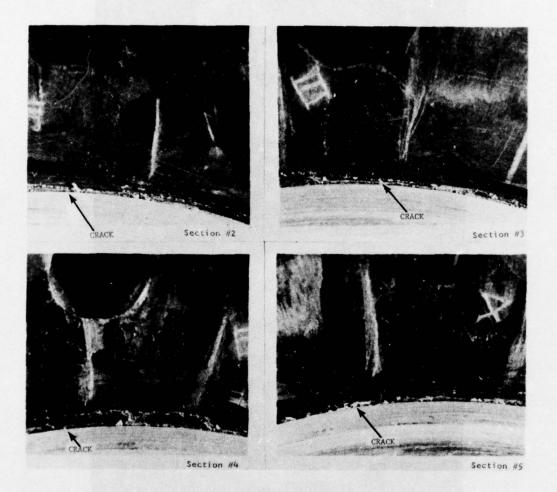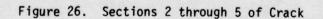
Figure 25. Section 1 of Crack and Scaling Objects

Figure 26. Sections 2 through 5 of Crack
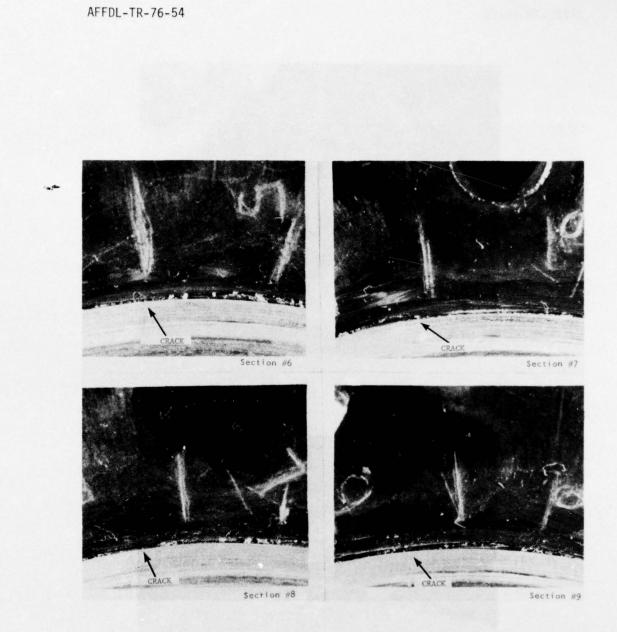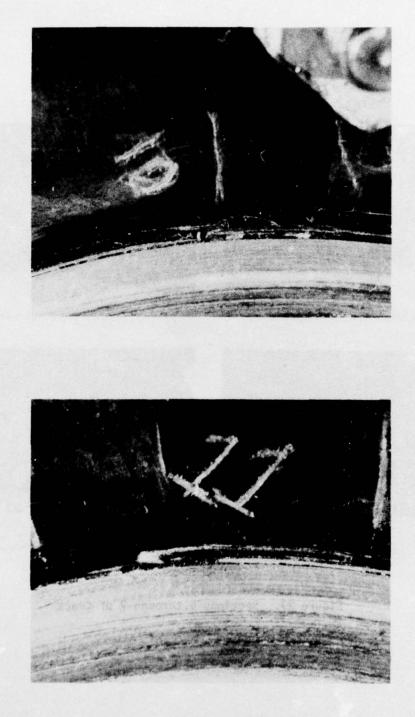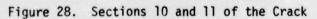
Figure 27. Sections 6 through 9 of Crack

Figure 28. Sections 10 and 11 of the Crack
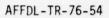
Figure 29. Close Up of a Typical Bolt Boss after 260 Miles
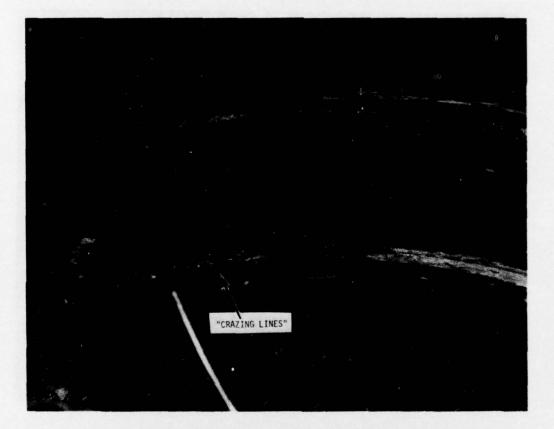
Figure 30.   Apparent "Crazing" Lines on the Outer Flange
of the Wheel

the bead seat of the outside flange of the wheel. Figure 31 shows an overall view of the wheel after 260 miles. The wear area on the Al hub is clearly visible in this picture.

After the examination of the wheel at 260 miles was complete, the roll test was continued. The wheel was disassembled and visually inspected at 10 mile increments for the next 40 miles. No further degradation of the wheel was found and so the tear down and visual inspection was performed at 20 mile increments for the next 40 miles. By this time a total of 340 miles had been put on the wheel. Next the wheel was run continuous for 60 miles, thoroughly inspected, and then run for 100 more miles. By this time a total of 500 miles had accumulated. Once again a thorough visual inspection was performed and a complete set of pictures taken. These photographs are shown in Figures 32 through 35.

After 650 miles of slow roll the amount of relative rotation between the Al hub and the wheel had increased. This was determined by visual inspection of match marks and the wear on the Al hub. Next a series of wires (Figure 36) were placed across the hub-wheel interface to determine the time, after wheel roll began, that relative hub rotation occurred and the direction and amount of the relative hub rotation. The wires were located and hooked up in such a manner that the direction of rotation would be indicated by an open circuit when the wires were tensioned and broke the soldered connection at the hub. Longer wires (with more slack) would cause open circuits later on as the hub continued to rotate relative to the wheel. Also a mechanism was located on the hub which would trip a signal each time the hub rotated past a certain point.

Figure 31. Overall View of Wheel after 260 Miles of
Dynamometer Slow Roll
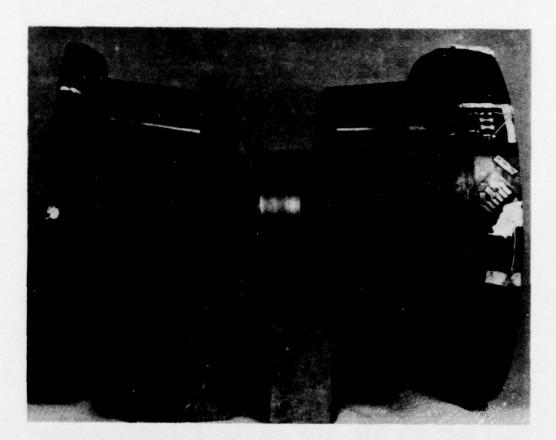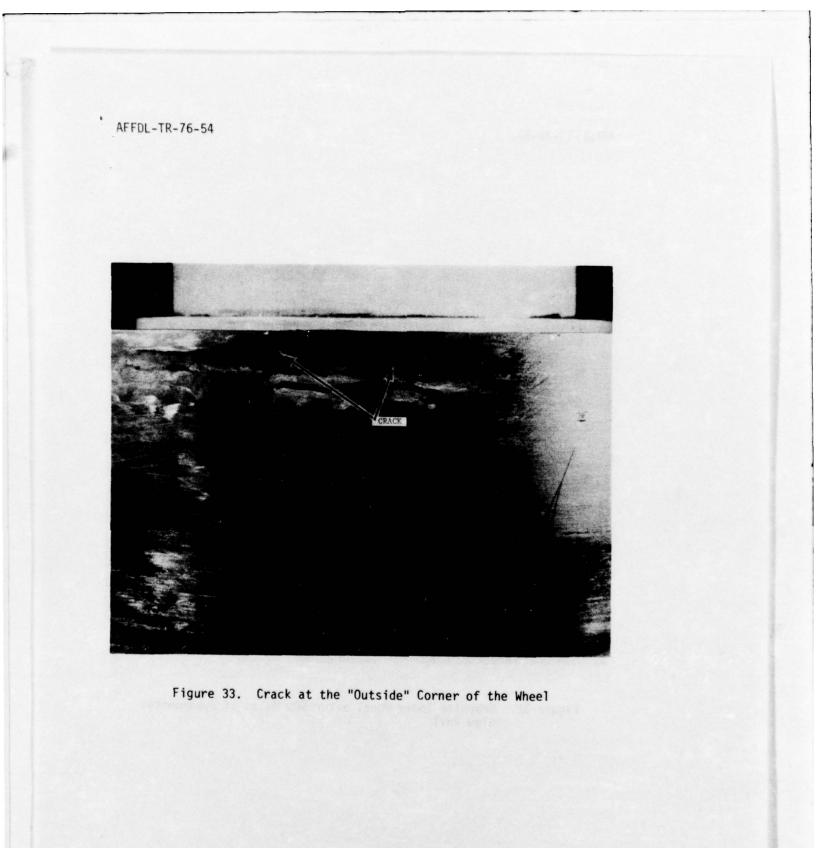
Figure 32. Graphite Epoxy Wheel after 500 Miles of Dynamometer
Slow Roll

Figure 33. Crack at the "Outside" Corner of the Wheel
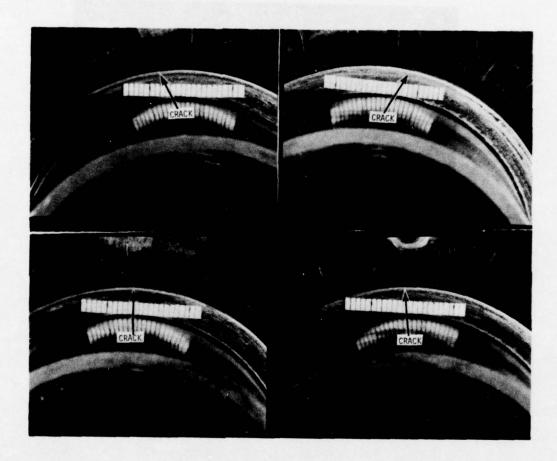
Figure 34.   View of the Crack next to the AL Hub
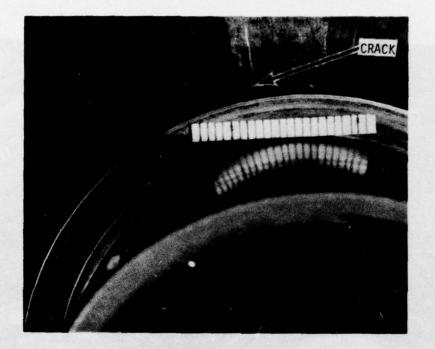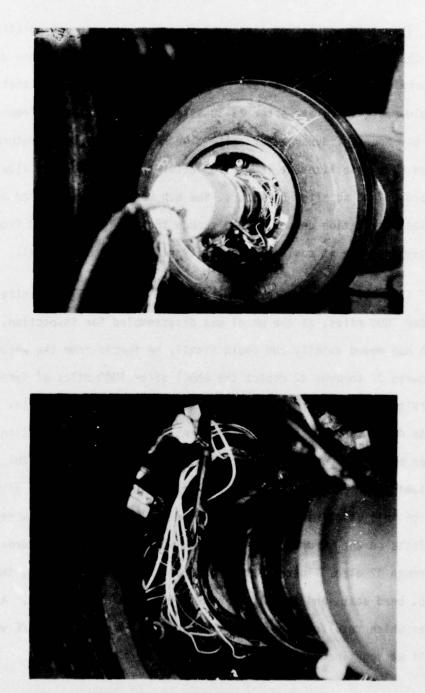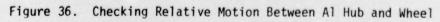
Figure 35.   View of the Crack next to the AL Hub

Figure 36. Checking Relative Motion Between Al Hub and Wheel

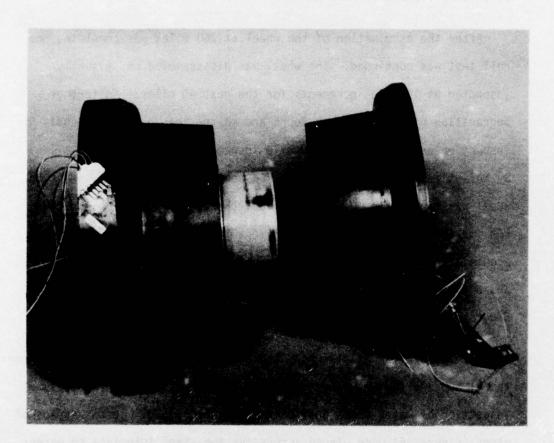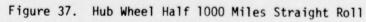This instrumentation disclosed that the hub made one rotation opposite to the wheel, about once every 1200 wheel revolutions. There are approximately 1000 wheel revs per mile. It was also noted that the hub would cease to rotate after 25-30 miles had been attained from start up or 5-7 hours of dynamometer roll. The contained air temperature of the bead seat stabilized at 150 - 170° after about one hour of slow roll start up and so after 6-7 hours, the hub most likely expanded enough that relative rotation ceased. Even though the hub had loosened from the epoxy adhesive it could not be easily removed from the wheel.

The roll test was uneventful from 650 to 1000 miles of straight roll. After 1000 miles, as the wheel was disassembled for inspection, the Al hub had moved axially and could finally be forced from the wheel. Figures 37 through 42 depict the wheel after 1000 miles of dynamometer straight roll. At this time the crack discovered at 650 miles had developed into definite corner delamination. As shown, this delamination extended over halfway around the circumference of the wheel. Since this delamination extended over halfway around the circumference of the wheel. Since this delamination did not extend into the hub of the wheel its effects on the structure of the wheel were negligible. Figures 37 through 42 also illustrate the condition of the bolt bosses, the wheel hub, bead seat, and the Al hub after 1000 mile of slow roll. All of the wear which resulted from the rubbing of the Al hub on the G/E wheel half was confined to the hub.

Figure 37. Hub Wheel Half 1000 Miles Straight Roll
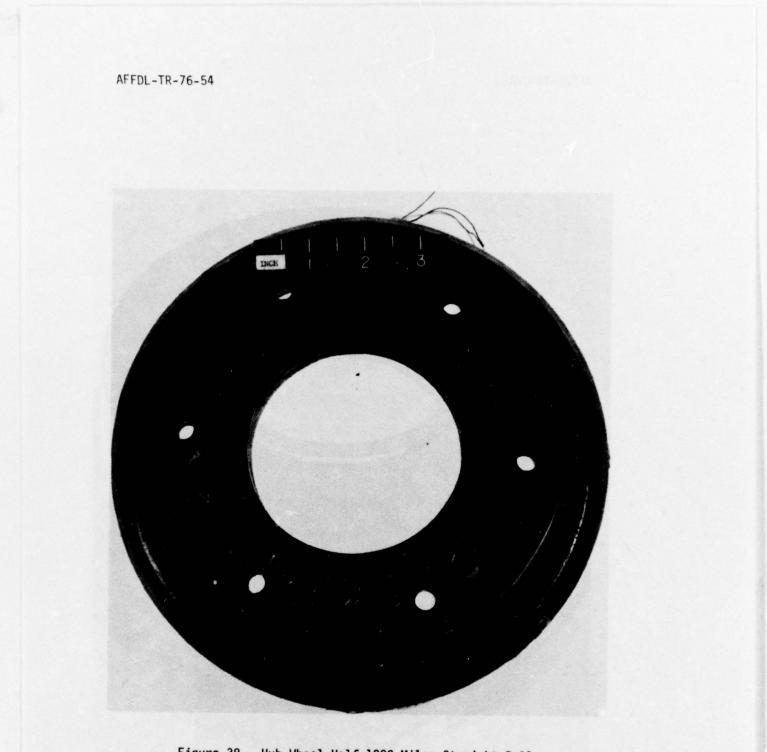
Figure 38. Hub Wheel Half 1000 Miles Straight Roll
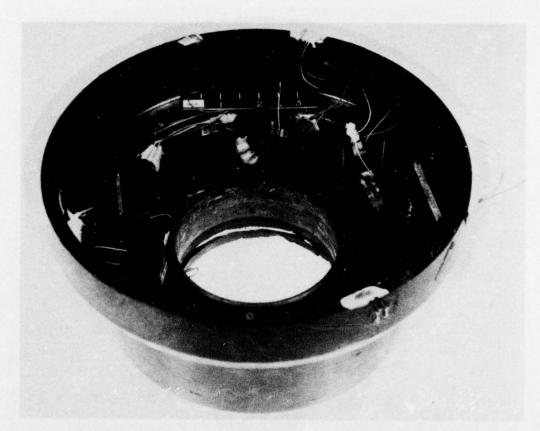
Figure 39. Hub Wheel Half 1000 Mile Straight Roll

Figure 40.   Hub Wheel Half 1000 Mile Straight Roll
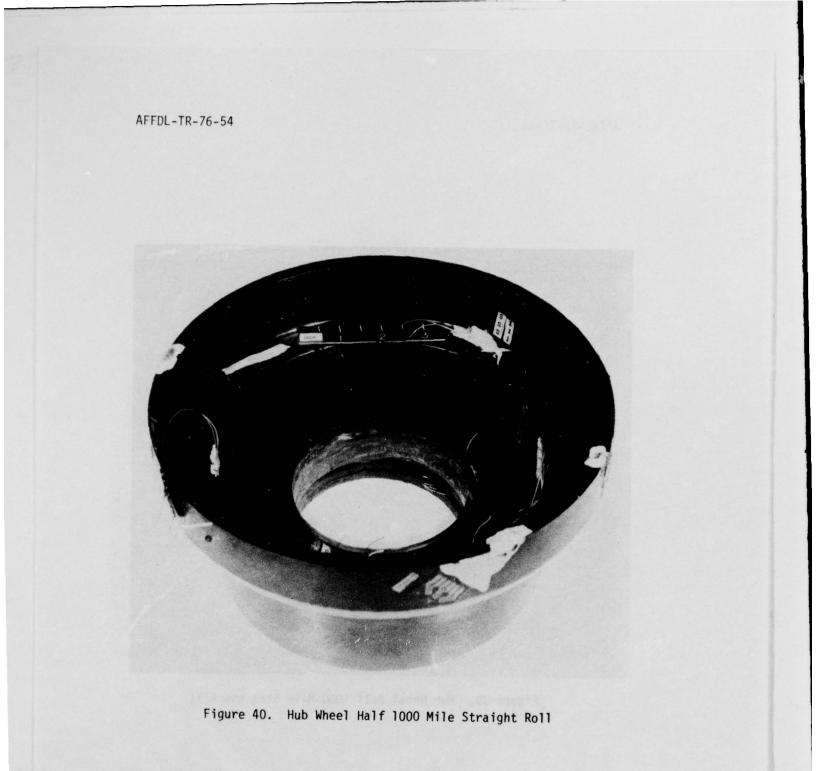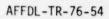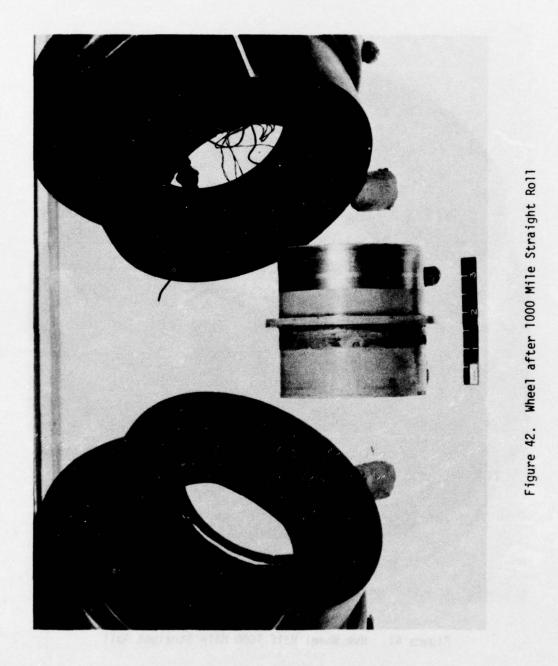
Figure 41. Hub Wheel Half 1000 Mile Straight Roll

Figure 42. Wheel after 1000 Mile Straight Roll
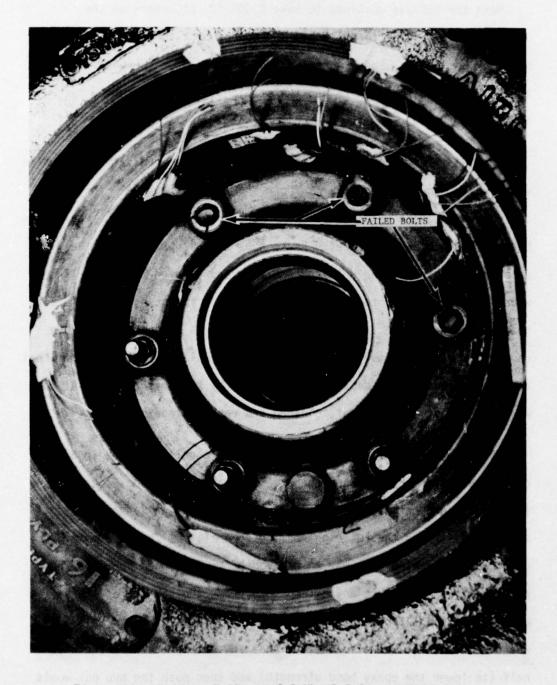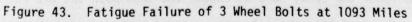
Next the hub was machined to have 0.004 in. clearance on the diameter with respect to the wheel and bonded back to the wheel using Hughson Chemical Co. Epoxy Adhesive, No. RD-1927-62. The wheel was then assembled with the tire and the straight roll test started again.

At 1093 miles into the straight roll tests a fatigue failure of three wheel bolts occurred and this is shown in Figure 43 and 44. This caused an immediate unbalanced load on the wheel and broke the epoxy bond between the hub and the wheel. As soon as the air pressure in the tire dropped, the dynamometer unlanded the tire and removed the load. The wheel bolts were only torqued to 15 ft-lbs (the torque requirements for the same bolts on the aluminum wheel are 25 ft-lb) and this must have caused the early fatigue failure. A close visual inspection of the wheel revealed no structural damage had been done by this mishap. The Al hub was pressed out of the wheel, cleaned and rebonded again.

The hub, unfortunately, was bonded to the wheel this time in a crooked position so that when the wheel was assembled (see Figure 45) there was a gap between the wheel halves. This gap was unacceptable since it destroyed the "O" ring sealing capability. Thus the major problem now was finding a way to remove the newly bonded hub from the wheel. It was felt that any attempts to press the hub out of the wheel might place too much side load on the structure and so this idea was discarded. It was also decided that any attempt to heat the wheel half (to lower the epoxy bond strength) and then push the hub out would be too risky. Finally the only alternative which seemed to remain was

Figure 43. Fatigue Failure of 3 Wheel Bolts at 1093 Miles
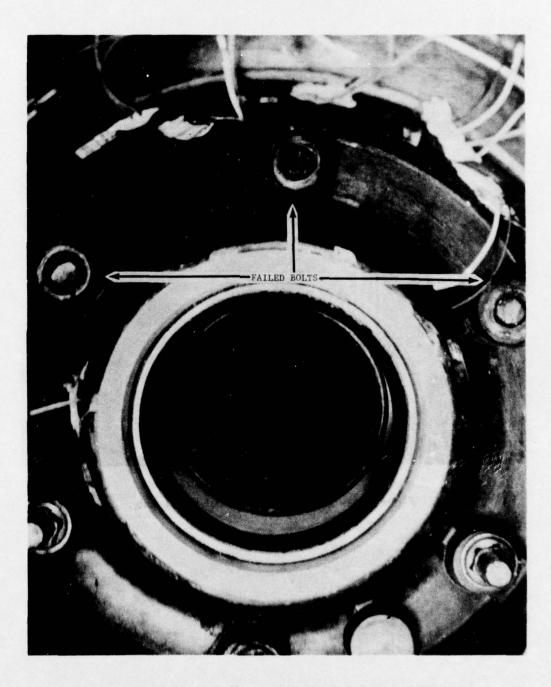
Figure 44. Fatigue Failure of 3 Wheel Bolts at 1093 Miles
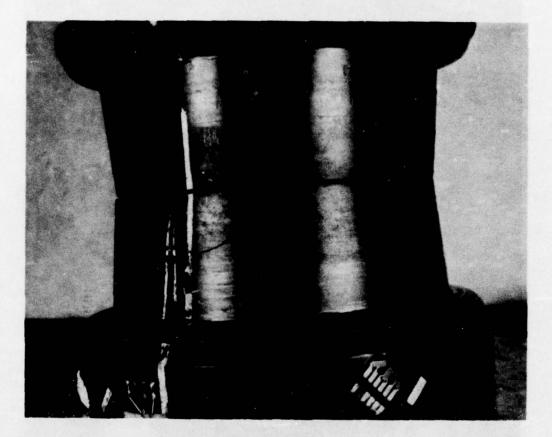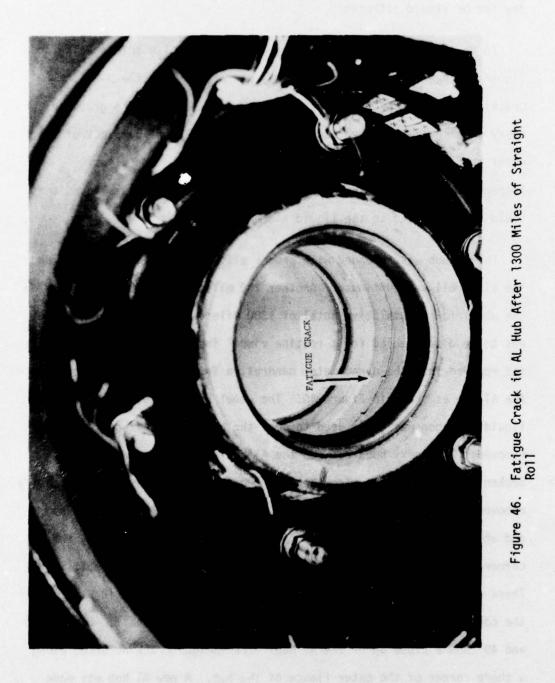
Figure 45. Effects of Crooked Wheel Hub
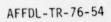
to break the adhesive bond by lowering the hub temperature by using dry ice or liquid nitrogen.

To do this, one end of the Al hub was covered with molding clay and liquid nitrogen (Boiling Point -320°F) was poured into the hub. A cracking noise was heard as the Al hub shrank away from the graphite epoxy wheel half. The hub was then tapped lightly and came out of the wheel half with very little applied force. A subsequent visual inspection of the wheel half was conducted and no damage was found that could be attributed to the liquid nitrogen soak.

The Al hub was rebonded with proper alignment to the wheel half and the slow roll was continued. Another 200 miles of slow roll were put on the wheel for a cumulative total of 1300 miles. At this time the wheel was to be disassembled for a routine visual inspection. When the wheel was removed from the dynamometer mandrel, a fatigue crack was found in the Al hub as shown in Figure 46. The wheel was then disassembled and liquid nitrogen was again used to cool the hub so that it could be removed. The epoxy bond between the Al hub and the wheel had also broken again sometime during the last 200 roll miles and so it was easily removed with the aid of the liquid nitrogen. Figure 47 shows the hub and wheel with the hub removed. Attempts had been made to epoxy the corner delamination (shown in Figures 37 to 42) to the wheel half. These attempts were only partially successful and as shown in Figure 47, the corner delamination had broken clear off the wheel half. Figures 48 and 49 show a close up of the Al hub. The fatigue crack occurred along a sharp corner of the outer flange of the hub. A new Al hub was made for the wheel with a thickened center wall and a chamfer which matched

59

Figure 46. Fatigue Crack in AL Hub After 1300 Miles of Straight Roll

FATIGUE CRACK
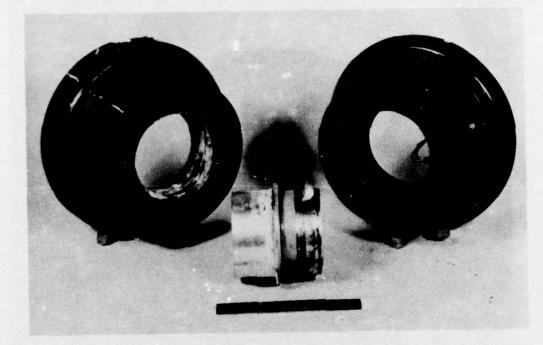
Figure 47. Wheel after 1300 Miles of Straight Roll
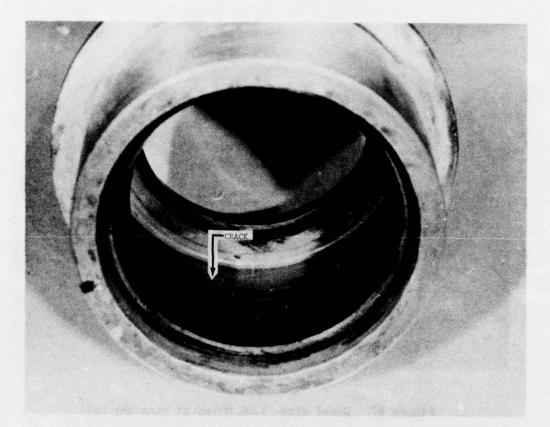
Figure 48. Crack in AL Hub after 1300 Miles Straight Roll
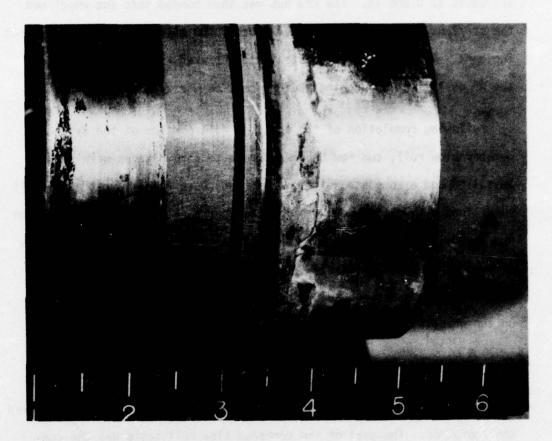
Figure 49. AL Hub after 1300 Miles Straight Roll

the delaminated wheel half. The half of this hub which was to be bonded was also knurled and the clearance between the hub and the wheel half increased to 0.006 in. The new hub was then bonded into the wheel and the straight roll test continued. Another 100 miles was attained without incident. This satisfied the straight, unbraked roll requirements of the AF qualification drawing (Reference 1 summarized in Chapter 2).

Following completion of the straight roll portion of the dyna-mometer slow roll, two new bead seat rosette strain gages were installed and a complete set of strain data were taken for straight roll conditions. Then the wheel was mounted in the camber roll configuration and a complete set of data were taken for camber slow roll. These data revealed there was essentially no increase in the magnitude of the magnitude of the strain due to the accumulated roll miles, at any point on the wheel. These data are presented in Section IV.

5. CAMBERED SLOW ROLL TESTS

The next test conducted was the dynamometer slow roll in the cambered configuration. The goal of the cambered slow roll tests was the com-pletion of 400 miles. Table 1 lists the significant events (tire failures) which occurred during these tests. None of these blow-outs did any damage to the wheel. Figure 50 illustrates three typical blown out tires.

TABLE 1

SUMMARY OF TIRE FAILURES FOR 15° CAMBERED SLOW ROLL TESTS

DATE	MILES/TIRE	TOTAL MILES	COMMENTS
8-12 June 1972	71.5	71.5	New Tire - "Slow" Blow-Out-Tire Sidewall Leaked Excessively
13-15 June 1972	105.3	176.8	New Tire - "Massive" Blow-Out
15-16 June 1972	54.2	231.0	New Tire - "Massive" Blow-Out
19-20 June 1972	67	298	New Tire - "Slow" Blow-Out
23-26 June 1972	38.5	336.5	New Tire - "Massive" Blow-Out
26 June 1972	19.1	355.6	New Tire - "Massive" Blow-Out
29 June 1972	44.4	400.0	Used Tire-Completed Tests O.K. Tire Still Good

The completion of the cambered slow roll tests was a major milestone for the wheel test in that all the unbraked slow roll requirements of the AF qualification drawing had been successfully completed. After the completion of the cambered slow roll tests another complete set of cambered slow roll strain data were attained.

6. HIGH SPEED TAKE OFF

The next test in this series involved the filming of one high speed take off and landing of the wheel. The wheel was placed on the dynamometer and subjected to a 6,000 lb straight load with a two minute 30 mph equivalent taxi roll followed by a 0 to 150 mph take off (accelerated at 10 ft/sec^2). A landing of the wheel was then performed at 4,600 lb straight load with

Figure 50. Typical Blow-Outs Sustained during 15° Cambered Slow
Roll Tests

touchdown at 90 mph. The landing was then followed by another two minute, 30 mph taxi roll. After these qualification tests, the wheel was disassembled and photographs were taken (Figures 51 through 53). These photographs show a certain amount of wear on the bolt bosses of each wheel half but the wear was judged to be reasonable, especially when considering the large number of times that the wheel had been assembled and disassembled. It is pointed out that the white material is only a protective epoxy coating which was applied over the strain gages. It was also noticed that the new Al hub was also beginning to show some signs of wear (see Figure 53). This indicates that the proper epoxy adhesive bond still had not been achieved. Also there was a region in the barrel of the wheel, directly over the "O" ring groove, that was beginning to crack slightly. This region was broken off when the "O" ring groove was machined and had, at that time, been bonded back to the wheel. Since the region is in compression, the effects of this cracking were negligible.

7.   INCREASED PRESSURE TESTS

The next tests involved pressurizing the wheel to 250 psi (twice rated pressure) and recording the strain data at 20 psi pressure increments. At approximately 240-250 psi the wheel emitted a cracking sound but continued to carry the load. A subsequent close visual inspection was conducted after the tire was deflated and the wheel disassembled but it did not reveal any evidence of structural damage.

Figure 51.   Wheel Half after 1400 Mile Straight Roll and 400 Mile
Camber Roll
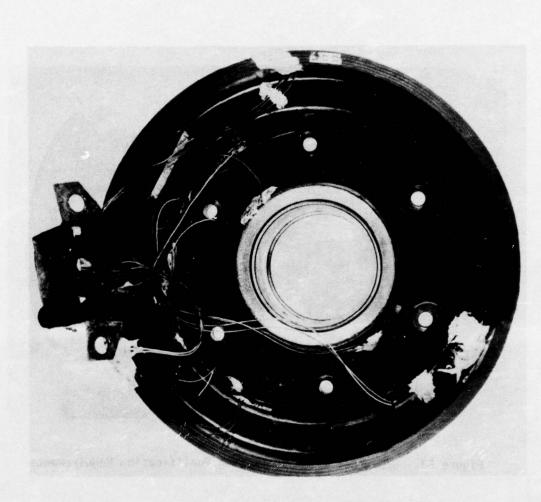
Figure 52. Hub Wheel Half after 1400 Mile Straight Roll and
400 Mile Camber Roll
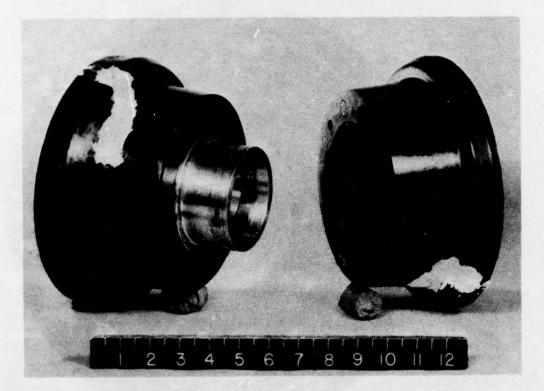
Figure 53. G/E Wheel after Completing Qualification Requirements

Next the wheel was inflated to rated pressure and strain data were taken for a straight slow roll at 50% overload (approximately 9,200 lbs radial load). As with the over-pressure loads, the strains measured were judged to be within the allowable limits (less than 4,000 micro-in/in) of the composite structure. The strain data for these tests are presented in Section IV.

8. CONTINUATION OF STRAIGHT ROLL TESTS

Following the over-pressurization tests and the overload slow roll tests, the straight roll at the rated load of 6,150 lbs, was started again. The wheel and tire assembly was torn down at approximately 200 mile intervals for a close visual inspection. The objective of the testing from this point on was to determine to actual number of straight roll miles that the graphite epoxy wheel could attain. After 400 additional straight roll miles the Al hub, once again, had loosened considerably and it was removed and rebonded.

Figures 54 through 56 illustrate the condition of the wheel at this point in the testing. Figure 55 shows the worst bolt boss of both wheel halves. As stated before, when consideration is made of the large number of times that the bolts had been tightened or removed, it is felt that these bosses were holding up well. Figure 56 shows the crack of the original secondary bond region above the "O" ring groove. Also as stated before, this area is in compression when the wheel is assembled and thus the effects of this crack are negligible.
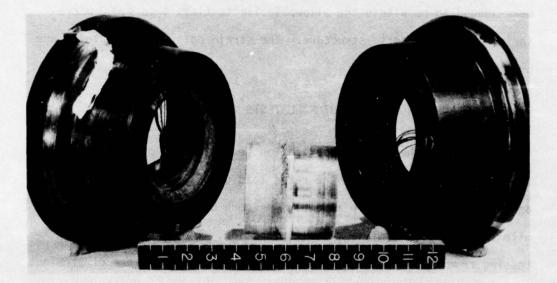
Figure 54. G/E Wheel after 1800 Mile Straight Roll 400 Mile
Camber Roll
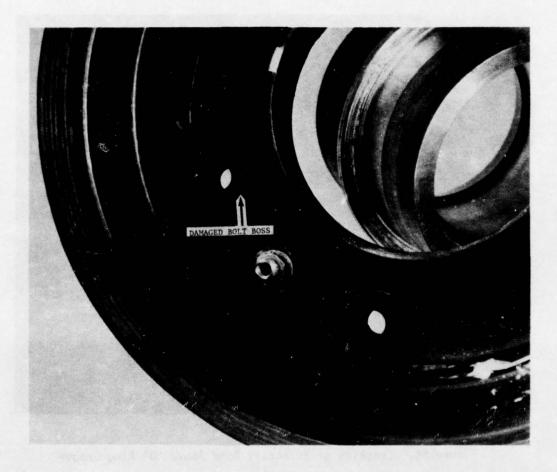
Figure 55. "Worst" Bolt Boss after 2200 Roll Miles
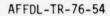
Figure 56. Cracking of Secondary Bond Above "O" Ring Groove

Figures 57 through 59 show the wheel after an additional 850 miles of straight roll. The crack in the barrel of the wheel (Figure 58) had widened slightly and a localized delamination (Figure 59) developed near one bolt hole. Neither of these defects caused the wheel to lose air and the wheel was visually inspected (on the dynamometer) every 20 to 30 miles. The tie bolts were changed about every 500 miles and after the tire had accumulated 1,270 miles the sidewall developed a void and it was necessary to install a new tire. The wheel was inspected closely during this teardown and no new defects were found. The straight roll tests were restarted and continued until the wheel had attained 1,712 miles. At this time, the wheel had been subjected to a total of 3,112 straight roll miles and 400 camber roll miles. Also, at this time, an air leak developed around the bottom of the air valve boss and the wheel began to lose air at a rapid rate. One of the bolts next to the valve stem broke off, apparently due to fatigue, and this must have caused, or at least contributed to, the air leak at the valve stem. Also when the nut end of the broken bolt was removed, part of the boss chipped off as shown in Figure 60. The wheel was disassembled for inspection purposes and it was found that the "O" ring had not slipped out of the groove. Thus, the air leakage was apparently caused by a defect that developed in the bond between the air valve and the graphite epoxy boss. This air leak was fixed by liberally applying an adhesive around the valve stem. Figure 61 shows an overall view of the same wheel half.
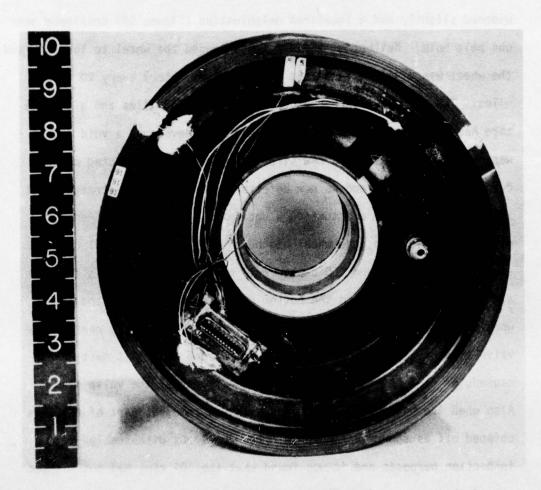
Figure 57.   Wheel after 400 Mile Camber Roll and 1400 Mile
Straight Roll
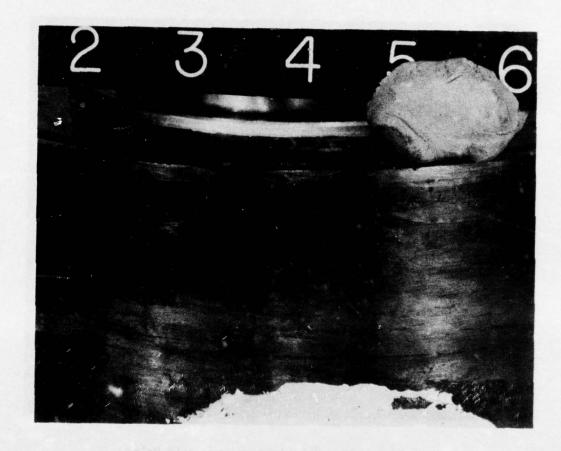
Figure 58. "Crack" in Barrel of Wheel
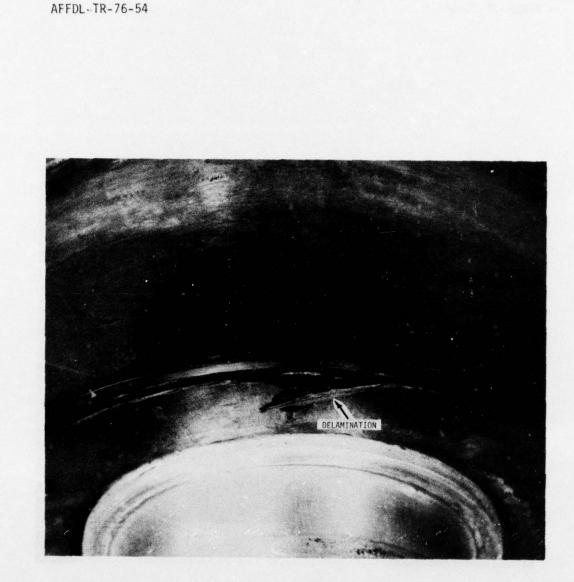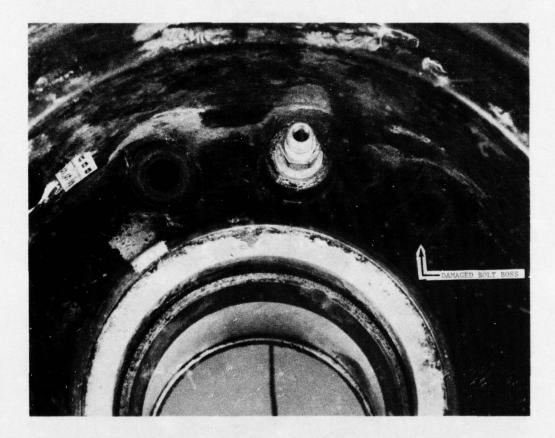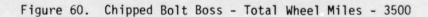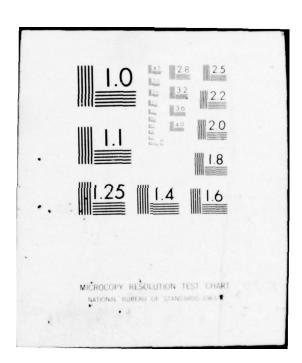
Figure 59.   Delamination near Bolt Hole

Figure 60. Chipped Bolt Boss - Total Wheel Miles - 3500

MICROCOPY RESOLUTION TEST CHART
NATIONAL BUREAU OF STANDARDS 1963
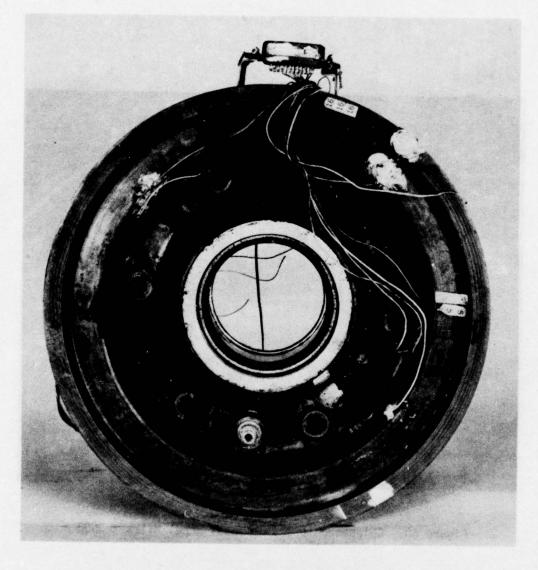
Figure 61.   Wheel Half after 3100 Miles of Straight Roll
and 400 Miles of Camber Roll

9.   DEVELOPMENT OF FATIGUE CRACKS AND PLANNED
      REPAIR AND INSPECTION TECHNIQUES

The straight roll tests continued until an additional 3,365 straight
roll miles had been accumulated above the required mileage. At this time,
a total of 4,765 straight roll miles and 400 camber roll miles had been
put on the wheel. At this time, the wheel once again began to rapidly
lose air. The wheel would still structurally withstand the loads from
the air pressure of 125 psi and it also withstood the rated straight load
of 6,150 lbs at the rated pressure but it would not hold the rated air
pressure. The wheel was sprayed with a soapy liquid used to help detect
air leaks and the results photographed as shown in Figures 62 through 64.
After close visual examination, small cracks were found in the bead seat
area and also at the bottom of the barrel of the wheel. These cracks
were circumferential in nature and extended clear around the wheel. The
cracks prevented the wheel from holding air but they did not weaken the
structure enough to cause failure. If a metal aircraft wheel had these
kinds of cracks, a catastrophic failure would be extremely likely to
happen. The graphite epoxy wheel, however, still withstood the structural
requirements even though these cracks prevented it from holding air.
The significance of these results is that fatigue failure with composite
wheels is not as likely to occur as with metal wheels and if the wheel
does have a fatigue failure, it is not likely to be catastrophic.

Since this wheel is a unique article, a series of inspection and repair
techniques will be undertaken in an attempt to repair the wheel. This
will include:

a. Ultrasonic "C"-Scan to see what patterns of the delaminations can
be recorded.
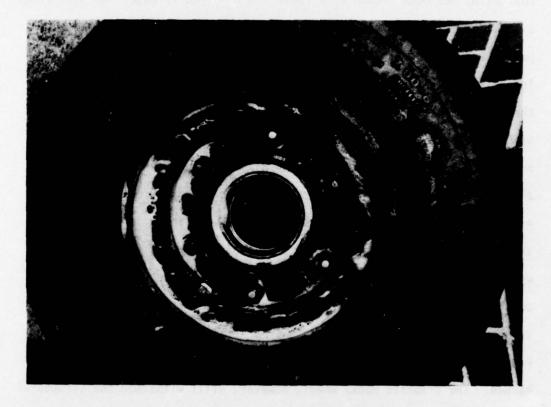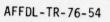
Figure 62. Air Leaks in Wheel
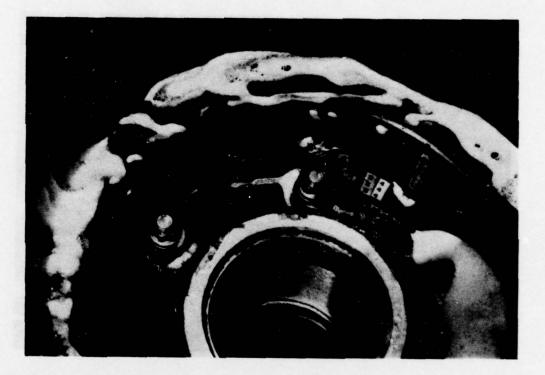
Figure 63.   Air Leaks at Bead Seat and Bottom of Barrel

Figure 64. Close Up of Air Leak in Bead Seat Area

b. Impregnate with XYGLO, photograph, and bake out.

c. Impregnate with Tetrabromoethane (TBE) for X-ray purposes.

d. X-ray for delaminations.

e. Bake out TBE.

f. X-ray for residue TBE.

g. Impregnate with epoxy in an attempt to repair the cracks.

h. Assemble with the tire and check for air leaks - repeat g as required.

i. Repeat ultrasonic "C"-Scan to see what patterns of the delaminations can be recorded.

j. Repeat impregnation with Tetrabromoethane (TBE) for X-ray purposes.

k. Structural test to the maximum extent possible.

l. Section, polish and photograph the pertinent cross sections.

The results of this effort will be documented in a subsequent technical report.

SECTION IV

PRESENTATION OF SIGNIFICANT DATA

This chapter will present selected strain data and comments about
these data. Strain data were taken for several load conditions from
12 rosette gages and 13 single gages. For convenience, the figures which
illustrate the strain gage locations are repeated again as Figures 65 and
66. A computer program was written which computed stresses from all the
strain data and then printed and plotted (Calcomp plotter) these data.
Separate plots were made for the strain and resulting stress data of
each strain gage. These data were reviewed and the highest strains and
stress are presented in this chapter.

Due to the anisotropic nature of the graphite epoxy structure, it
was necessary to make certain simplifying assumptions in order to compute
stresses from the strains. These assumptions are discussed in Subsection 1.
The computed stresses were compared to the maximum-strain failure criteria.
This criteria is discussed in Subsection 2. The rest of the chapter
discusses the instrumentation, method of data collection, and the data
obtained. Appendix 1 contains a sampling of the data obtained from each
strain gage.

1. LAMINATION THEORY USED TO COMPUTE STRESSES

a. Basic Engineering Constants and Notation

The engineering constants (Young's modulii, Poisson's ratios and
shear modulii) that are presently most accurate for use with composite
materials analysis are those which have been determined experimentally.

86
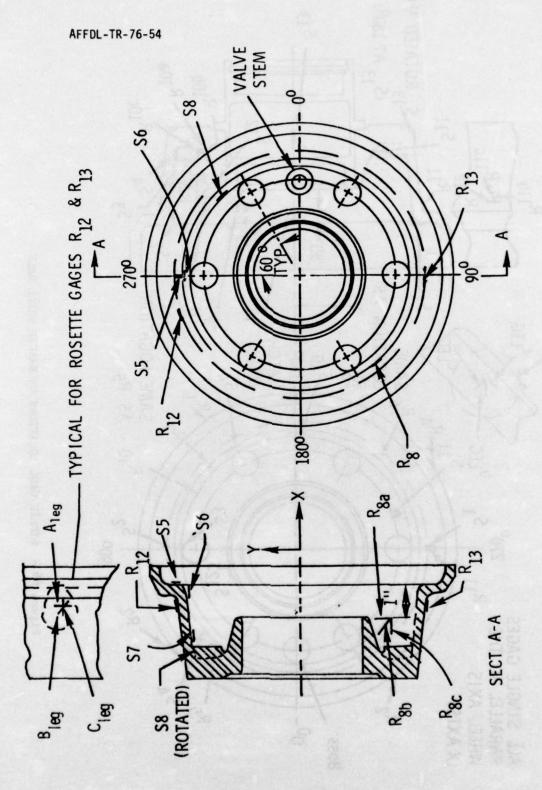
Figure 65 – STRAIN GAGE LOCATIONS ON NON-BRAKE WHEEL HALF
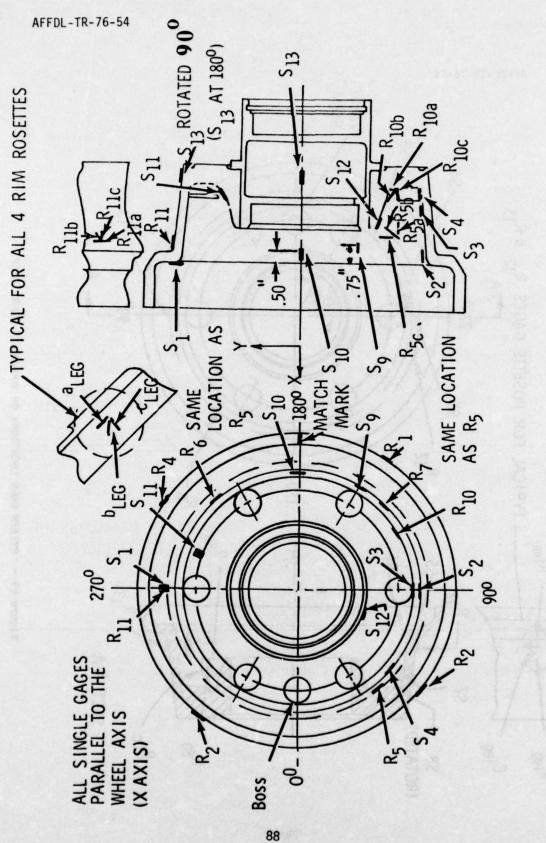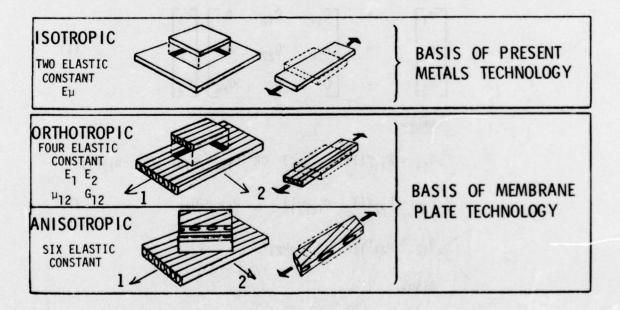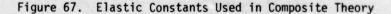
Figure 66 - STRAIN GAGE LOCATIONS ON BRAKED WHEEL HALF

88

Figure 67 illustrates the terminology and number of engineering
constants applicable to two dimensional composite lamina. The 1-2 axes
notation will be used for the lamina with the 1 axis parallel to the
fiber and the 2 axis perpendicular to the fiber. This coordinate
notation may also be referred to as the lamina natural axes. The
present accepted practice is to experimentally determine a fundamental
engineering constant of a lamina and then using lamination theory,
analytically predict the engineering constants of a laminate.
(References 3 and 4).

Figure 67. Elastic Constants Used in Composite Theory

Four lamina engineering constants are readily obtainable on an experimental basis. As shown in Figure 67, these are E_1, E_2, and μ_{12} and G_{12}. These constants are valid for a two dimensional orthotropic material subjected to in-plane loading. Thus, when loaded (see Figure 67) the orthotropic lamina does not rotate about any axis. Instead the lamina deformation is restricted to translation along the natural axes. At the present time, the experimental determination of more than four lamina engineering constants is not a common practice. For an orthotropic lamina, stress is related to strains by: (Reference 3)

$$\begin{bmatrix} \sigma_1 \\ \sigma_2 \\ \sigma_3 \end{bmatrix} = \begin{bmatrix} Q_{11} & Q_{12} & 0 \\ Q_{12} & Q_{22} & 0 \\ 0 & 0 & Q_{66} \end{bmatrix} \begin{bmatrix} \varepsilon_1 \\ \varepsilon_2 \\ \varepsilon_3 \end{bmatrix} \qquad (1)$$

Where:

$$Q_{11} = E_{11}/(11 - \mu_{12}\mu_{21}) \quad \text{OR} \quad Q_{12} = \mu_{12}E_{22}/(1 - \mu_{12}\mu_{21})$$

$$Q_{22} = E_{22}/(1 - \mu_{12}\mu_{21}) \qquad Q_{66} = G_{12} \qquad (2)$$

$$Q_{12} = \mu_{21}E_{11}/(1 - \mu_{12}\mu_{21})$$

Also:

$$\mu_{21}E_{11} = \mu_{12}E_{22}$$

The wheel is composed of many lamina laid up in 0°, ± 45° and 90° orientations as shown in Figure 68. The axis notation to be used for the laminate in the wheel is also shown in Figure 68. Thus, the wheel revolves about the X axis and the Y axis is in the hoop direction. Also,

STATION

LAYER #	A	B	C	D	E	F	G	H	I	J	K
1			4CIRC		3CIRC		6CIRC				
2			3 R/A		2 R/A		4 R/A				
3			4CIRC		3CIRC		6CIRC				
4			3 R/A		2 R/A		4 R/A				
5			4±45		2±45		6±45				
6			4CIRC		3CIRC		6CIRC				
7			2 R/A		1 R/A		4 R/A				
8			4±45		4±45		4±45				
9			4CIRC		3CIRC		6CIRC				
10			2 R/A		1 R/A		4 R/A				
11			4±45		2±45		6±45				
12			4CIRC		3CIRC		6CIRC				
13	3 R/A		2 R/A		1 R/A		4 R/A				
14	5CIRC		4CIRC		3CIRC		6CIRC				
15								.2 R/A			
16								2±45			
17								3CIRC			
18								1 R/A			
19								2±45			
20								4CIRC			
21								4 R/A			
22								4CIRC			
23								4 R/A			
24								4CIRC			
AS REQD								ETC.			

TAPER
SEE SKETCH
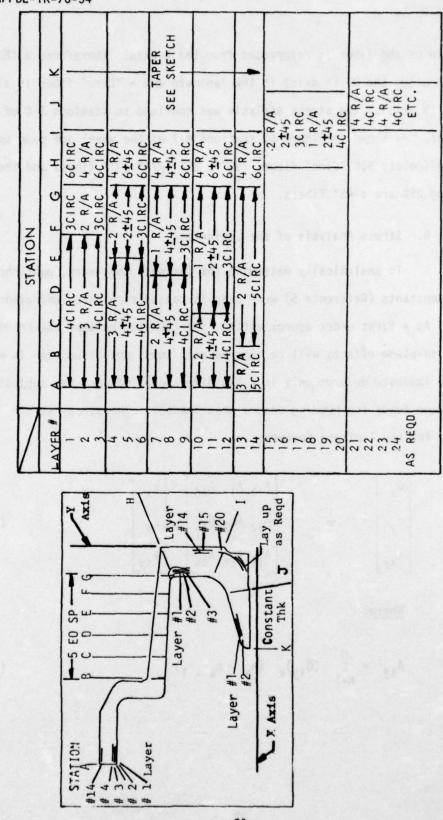
Figure 68 – WHEEL LAMINATE DESCRIPTION

the angle of the fiber is referenced from the X axis. Therefore, a "R/A" fiber is along the 0° (X axis) in the laminate and a "Circ" fiber is along the 90° (Y axis). The stress analysis was confined to stations A-G of the wheel. As shown in Figure 68 stations A-I of the wheel are made up of approximately 50% "Circ" fibers (90°), 25% "R/A" (0°) fibers and the remaining 25% are ± 45° fibers.

b. Stress Analysis of the Laminate

To analytically determine the laminate constants, published lamina constants (Reference 5) were used in conjunction with lamination theory. As a first order approximation, the coupling between the bending and the in-plane effects will be ignored and, thus, the assumption is made that the laminate deforms only in a two dimensional manner when subjected to in-plane loads (no bending occurs when loaded). The stress strain equation for the laminate becomes:
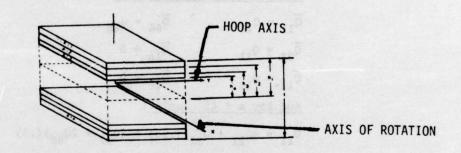
$$
\begin{bmatrix} \sigma_x \\ \sigma_y \\ \tau_{xy} \end{bmatrix} = \frac{1}{t} \begin{bmatrix} A_{11} & A_{12} & A_{16} \\ A_{12} & A_{22} & A_{26} \\ A_{16} & A_{26} & A_{66} \end{bmatrix} \begin{bmatrix} \varepsilon_x \\ \varepsilon_y \\ \lambda_{xy} \end{bmatrix}
\tag{3}
$$

Where:

$$
A_{ij} = \sum_{k=1}^{\eta} (\overline{Q}_{ij})_k (h_k - h_{k-1})
\tag{4}
$$
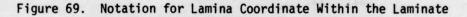
Figure 69 denotes the notation used for the Equations 3, 4 and 5. The stiffness ($\overline{Q}_{ij}$) terms are the constants found for the orthotropic lamina natural axes (Q_{ij}) that have been rotated to the X-Y coordinate system of the wheel.

Figure 69. Notation for Lamina Coordinate Within the Laminate

The transformation of the Q_{ij} constants is done by using:

$$\overline{Q}_{11} = Q_{11}\cos^4\theta + 2(Q_{12} + 2Q_{66})\sin^2\theta\cos^2\theta + Q_{22}\sin^4\theta$$

$$\overline{Q}_{22} = Q_{11}\sin^4\theta + 2(Q_{12} + 2Q_{66})\sin^2\theta\cos^2\theta + Q_{22}\cos^4\theta$$

$$\overline{Q}_{12} = (Q_{11} + Q_{22} - 4Q_{66})\sin^2\theta\cos^2\theta + Q_{12}(\sin^4\theta + \cos^4\theta) \qquad (5)$$

$$\overline{Q}_{66} = (Q_{11} + Q_{22} - 2Q_{12} - 2Q_{66})\sin^2\theta\cos^2\theta + Q_{66}(\sin^4\theta + \cos^4\theta)$$

$$\overline{Q}_{16} = (Q_{11} - Q_{12} - 2Q_{66})\sin\theta\cos^3\theta + (Q_{12} - Q_{22} + 2Q_{66})\sin^3\theta\cos\theta$$

$$\overline{Q}_{26} = (Q_{11} - Q_{12} - 2Q_{66})\sin^3\theta\cos\theta + (Q_{12} - Q_{22} + 2Q_{66})\sin\theta\cos^3\theta$$

Substituting the Q_{ij} values for the natural lamina into the above equations gives (note that $\overline{Q}_{11}$ is along the X axis and $\overline{Q}_{22}$ is along the Y axis).

For a 0° Lamina (R/A):

$$\overline{Q}_{11} = Q_{11} \qquad\qquad \overline{Q}_{66} = Q_{66}$$

$$\overline{Q}_{22} = Q_{22} \qquad\qquad \overline{Q}_{16} = 0$$

$$\overline{Q}_{12} = Q_{12} \qquad\qquad \overline{Q}_{26} = 0$$

and for a 90° lamina (CIRC):

$$\overline{Q}_{11} = Q_{22} \qquad\qquad \overline{Q}_{66} = Q_{66}$$

$$\overline{Q}_{22} = Q_{11} \qquad\qquad \overline{Q}_{16} = 0$$

$$\overline{Q}_{12} = Q_{12} \qquad\qquad \overline{Q}_{26} = 0$$

and for a + 45° lamina:

$$\overline{Q}_{11} = (Q_{11} + Q_{22})(.25) + (Q_{12} + 2Q_{66})(.5)$$

$$\overline{Q}_{22} = \overline{Q}_{11}$$

$$\overline{Q}_{12} = (Q_{11} + Q_{22} - 4Q_{66})(.25) + (Q_{12})(.5)$$

$$\overline{Q}_{66} = (Q_{11} + Q_{22} - 2Q_{12} - 2Q_{66})(.25) + Q_{66}(.5)$$

$$\overline{Q}_{16} = (Q_{11} - Q_{12} - 2Q_{66})(.25) + (Q_{12} - Q_{22} + 2Q_{66})(.25)$$

$$\overline{Q}_{26} = \overline{Q}_{16}$$

for a (-45°) lamina:

$$\overline{Q}_{11} = (Q_{11} + Q_{22})(.25) + (Q_{12} + 2Q_{66})(.5)$$

$$\overline{Q}_{22} = \overline{Q}_{11}$$

$$\overline{Q}_{12} = (Q_{11} + Q_{22} - 4Q_{66})(.25) + (Q_{12})(.5)$$

$$\overline{Q}_{66} = (Q_{11} + Q_{22} - 2Q_{12} - 2Q_{66})(.25) + Q_{66}(.5)$$

$$\overline{Q}_{16} = - (Q_{11} - Q_{12} - 2Q_{66})(.25) - (Q_{12} - Q_{22} + 2Q_{66})(.25)$$

$$\overline{Q}_{26} = \overline{Q}_{16}$$

The above equations reveal that for a 0° and 90° lamina, $\overline{Q}_{16} = \overline{Q}_{26} = 0$. Also if for every lamina of a +45° orientation there is another lamina of -45° orientation with the same orthotropic properties and thickness, (true in this case because the same pre-preg was used throughout)

94

the $\bar{Q}_{16}$ and $\bar{Q}_{26}$ terms will have the same absolute magnitude but opposite sign. Since $\bar{Q}_{16} = \bar{Q}_{26} = 0$ for the 0° and 90° lamina, the only contributions to the A_{16}, A_{26} terms of Equation 3 above are the $\bar{Q}_{16}$, $\bar{Q}_{26}$ terms for the ± 45° lamina. Thus if equal numbers of ± 45° lamina are used, the sum of the A_{16} and A_{26} terms for the laminate will equal zero. Therefore, Equation 3 becomes:

$$\begin{bmatrix} \sigma_x \\ \sigma_y \\ \tau_{xy} \end{bmatrix} = \frac{1}{t} \begin{bmatrix} A_{11} & A_{12} & 0 \\ A_{12} & A_{22} & 0 \\ 0 & 0 & A_{66} \end{bmatrix} \begin{bmatrix} \varepsilon_x \\ \varepsilon_y \\ \gamma_{xy} \end{bmatrix} \tag{6}$$
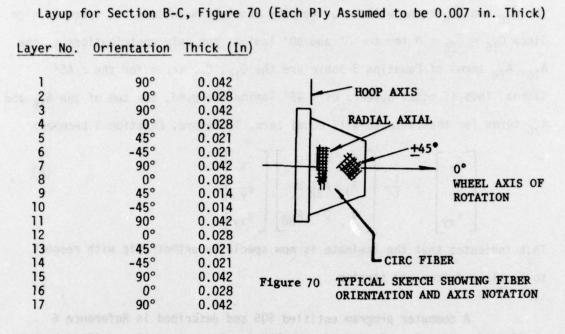
This indicates that the laminate is now specially orthotropic with respect to in-plane forces and strains.

A computer program entitled SQ5 and described in Reference 6 was used to obtain the laminate constants. This program defines the limit stress interaction diagram as discussed in Subsection 2. The inputs required for this program are the lamina constants, the limit allowable strains of the lamina, and the layup used to construct the laminate.

Inputs to SQ5 for Modmor II with 4617 Resin (Reference 5)

2 (Perpendicular to Fiber)

1

Basic Lamina
(Parallel to Fiber)

Lamina Constants

$\varepsilon_1 = 20 \times 10^6$ psi

$\varepsilon_2 = 2.1 \times 10^6$ psi

$\mu_{12} = 0.21$

$G_{12} = 0.85 \times 10^6$ psi

Limit Allowable Strains of Basic Lamina

ε_1 COMP (-0.0066) ε_1 TEN (0.0058)

ε_2 COMP (-0.0067) ε_2 TEN (0.0025)

γ_{12} COMP (-0.01) γ_{12} TEN (0.01)

Layup for Section B-C, Figure 70 (Each Ply Assumed to be 0.007 in. Thick)

Layer No.	Orientation	Thick (In)
1	90°	0.042
2	0°	0.028
3	90°	0.042
4	0°	0.028
5	45°	0.021
6	-45°	0.021
7	90°	0.042
8	0°	0.028
9	45°	0.014
10	-45°	0.014
11	90°	0.042
12	0°	0.028
13	45°	0.021
14	-45°	0.021
15	90°	0.042
16	0°	0.028
17	90°	0.042

Figure 70   TYPICAL SKETCH SHOWING FIBER ORIENTATION AND AXIS NOTATION

Note from Figure 68 that the layup differs slightly from Sections A to I. To take this into account, the SQ5 program was run for three different positions, Sections B-C, F-G, and G-I. The SQ5 output included the (A/T) matrix (see Equation 6) and the average elastic constants for the laminate (E_x, E_y, μ_{xy}, G_{xy}). The values of these constants obtained from Sections F-G and G-I were within 5% of the values obtained for Section B-C, consequently Section B-C was chosen to be the typical laminate for the wheel cross section.

An inspection of Equations 5 and 1 above shows that the laminate stress-strain equation is essentially of the same form as the lamina stress-strain equation. This indicates that due to the ply layup and the assumption that no laminate bending occurs, the laminate

96

has the same governing relationship as the lamina. Thus, given E_x, E_y, μ_{xy} and G_{xy} for the laminate, one can also use Equation 1 with similar equations:

$$Q_{11} = Q_{xx} = E_{xx}/(1 - \mu_{xy}\mu_{yx})$$

$$Q_{22} = Q_{yy} = E_{yy}/(- \mu_{xy}\mu_{yx})$$

$$Q_{12} = Q_{xy} = \mu_{yx}E_{xx}/(1 - \mu_{xy}\mu_{yx}) = \mu_{xy} E_{yy}/(1 - \mu_{xy}\mu_{yx})$$

$$Q_{66} = G_{xy} \text{ and } \mu_{yx}E_{xx} = \mu_{xy}E_{yy}$$

(7)

To obtain:

$$\begin{bmatrix} \sigma_x \\ \sigma_y \\ \tau_{xy} \end{bmatrix} = \begin{bmatrix} Q_{xx} & Q_{xy} & 0 \\ Q_{xy} & Q_{yy} & 0 \\ 0 & 0 & Q_{66} \end{bmatrix} \begin{bmatrix} \varepsilon_x \\ \varepsilon_y \\ \gamma_{xy} \end{bmatrix}$$
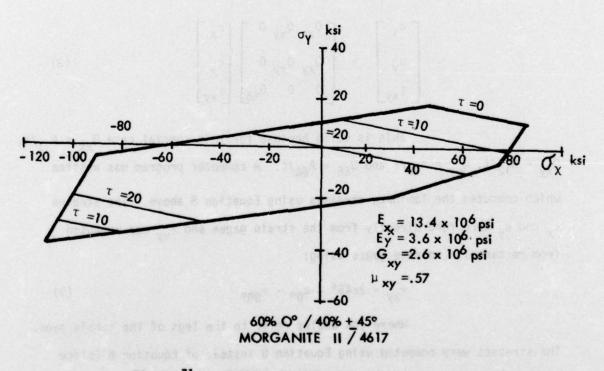
(8)

This is valid because for this special case $Q_{xx} = A_{11}/t$, $Q_{xy} = A_{12}/t$, $Q_{yy} = A_{22}/t$ and $Q_{66} = A_{66}/t$. A computer program was written which computed the laminate stresses using Equation 8 above. The strains ε_x and ε_y were read directly from the strain gages and γ_{xy} was computed from rectangular rosette gages using:
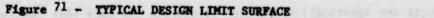
$$\gamma_{xy} = 2\varepsilon 45° - \varepsilon_{0°} - \varepsilon_{90°}$$

(9)

Where the angles refer to the legs of the strain gage. The stresses were computed using Equation 8 instead of Equation 6 (since both are identical) to further illustrate the fact that the laminate elastic response has been greatly simplified.

2. CRITERIA USED TO COMPUTE LIMIT ALLOWABLE STRESSES

The SQ5 computer program was used to determine the limit allowable stresses interaction diagram for the wheel. This program uses limit allowable lamina strains and the maximum allowable strain criteria to compute the coordinates for the limit allowable stress interaction diagram. A typical limit stress interaction diagram is shown in Figure 71. The maximum allowable strain criteria simply means that the computed lamina strains must not exceed the limit lamina strain allowables which are input to the program.

$E_{xx} = 13.4 \times 10^6$ psi
$E_y = 3.6 \times 10^6$ psi
$G_{xy} = 2.6 \times 10^6$ psi
$\mu_{xy} = .57$

60% 0° / 40% + 45°
MORGANITE II / 4617

Figure 71 - TYPICAL DESIGN LIMIT SURFACE

To determine all possible combinations of the laminate allowable stresses
(and thus the interaction diagram), the SQ5 program proceeds as follows:

(1. All combinations of unit allowable stresses (tension and
compression combinations) are individually applied to the laminate.

(2. Using an inverse form of the equivalent of Equation 8,
the laminate strains (ϵ_x, ϵ_y, γ_{xy}) are determined for all these combinations.

(3. These strains are then rotated to the lamina axes and thus
the lamina strains, ϵ_1, ϵ_2, and γ_{12} are determined. The lamina strains
can now be compared to the limit allowable lamina stresses which were
input to the program.

(4. Since these lamina strains are produced by unit laminate
stresses, the maximum allowable laminate stresses can be determined by
the ratio:

$$\left[\frac{\text{Limit Allowable Lamina Strain}}{\text{Lamina Strain Due to Unit Laminate Stress}} \right] \times (\text{Unit Laminate Stress})$$

(5. The maximum allowable shear stress is then determined
using this ratio. Next, the SQ5 computes shear stress increments of
±10,000 psi from zero shear stress to the maximum allowable shear stress.

(6. σ_x and σ_y intercepts are then computed and printed out for
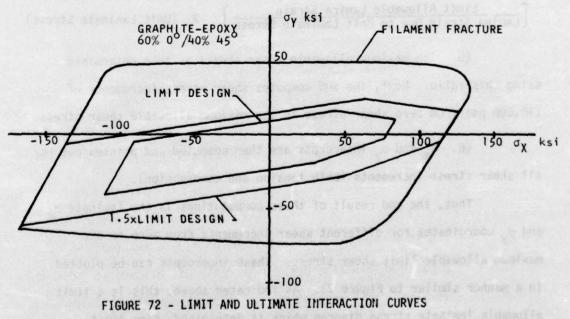all shear stress increments (both tension and compression).

Thus, the end result of these computations is the laminate σ_x
and σ_y coordinates for different shear increments from zero to the
maximum allowable limit shear stress. These incercepts can be plotted
in a manner similar to Figure 71. As indicated above, this is a limit
allowable laminate stress diagram which is determined using limit

99

allowable lamina strains. These limit allowable lamina strains have been
computed by appropriate reductions of the experimentally determined
ultimate $\pm\varepsilon_1$, $\pm\varepsilon_2$, and $\pm\gamma_{12}$ strains. Thus, if the wheel stresses, as
computed from the strain gage data, fall within the confines of the limit
interaction stress diagram then none of the lamina strains have exceeded
the limit allowable values.

This criteria is considered to be quite conservative. However,
an accurate analytical prediction of ultimate allowable laminate stresses
requires the use of nonlinear techniques or finite element analyses. A
sample ultimate stress curve is shown in Figure 72. This curve is for
the same laminate used in Figure 71. Thus, the limit interaction curves of
Figure 71 and Figure 72 are identical. These curves are shown to
illustrate the nonlinear relationship between the limit design allowables
and actual lamina fracture.

FIGURE 72 - LIMIT AND ULTIMATE INTERACTION CURVES

The limit stress interaction diagram for the wheel is presented in Subparagraph IV-7.

3.   INSTRUMENTATION

Strain data were taken from the wheel during pressurization and both straight and camber slow roll conditions. To obtain the data during pressurization, a null-balance wheatstone-bridge circuit was constructed using a strain indicator, temperature compensating strain gages, and the strain gages on the wheel. The temperature compensating gages were placed on a unidirectional laminate which was ten plies thick. To match the thermal expansion properties as closely as possible, three temperature compensating gages were used, one along the fiber, one at 45° to the fiber, and one transverse to the fiber direction. This required switching from circuit to circuit in order to match the temperature compensating gage to the gage being read. The switches used were frequently checked for signal variation due to poor (dirty) contacts, and cleaned, when necessary, to maintain good contact. The zero for all strain readings was taken with the wheel in the disassembled state. This zero was rechecked almost every time the wheel was taken apart. Discussion of the zero drift and various strain reading anomalies which occurred is presented in Subparagraphs 4 through 6.

A light-beam oscillograph was used to record the strain data taken during the camber and straight slow roll. Three channels of data were simultaneously recorded. Initially, the data were transmitted through a long cable to the recorder. This cable was allowed to "wind-up" around the wheel for 3 or 4 revolutions and then the wheel was unlanded and returned to its original position. Later in the tests, a slip ring

101

was used to transmit the data. Calibration of the oscillograph was done by shunting a known change of resistance (strain) across the circuit and observing the corresponding deflection of the light beam. For reference purposes, the wheel was divided into four quadrants (see Figures 65 and 66 with the 0° orientation mark placed at the valve stem. The recording system was set up so that a "blip" would be registered by the oscillograph every time the valve stem (0°) was directly over the load. The oscillograph paper was then developed and readings were taken for one complete cycle. These data were then punched on computer cards for use as input to the computer program that was written to compute and plot the strains and stresses.

4. STRAINS AND STRESSES FOR PRESSURIZATION

The zero for the strain gages was established with the wheel disassembled. The tire seated against the rim at 20 psi, therefore the first strain readings were taken at this pressure. Strain data were then taken at 10 psi pressure increments from 20 psi to 130 psi. Repetitions of all pressure increments were conducted before the data were recorded. The wheel was allowed to remain at 50 psi for 3 1/2 hrs, at 80 psi for 1 1/2 hrs, and 130 psi for approximately 70 hrs. Pressure readings and strains were read before and after these periods. No pressure loss was observed at 50 and 80 psi and approximately 10 psi was lost from 130 psi over 70 hours. The tire was inflated again to 130 psi and allowed to stabilize for approximately 1 hour before the strains were read. Some of the changes in strain observed over these three periods must be attributed to the inaccuracy of the Wheatstone Bridge circuit used and some must be attributed to the stretching of the tire, which may have
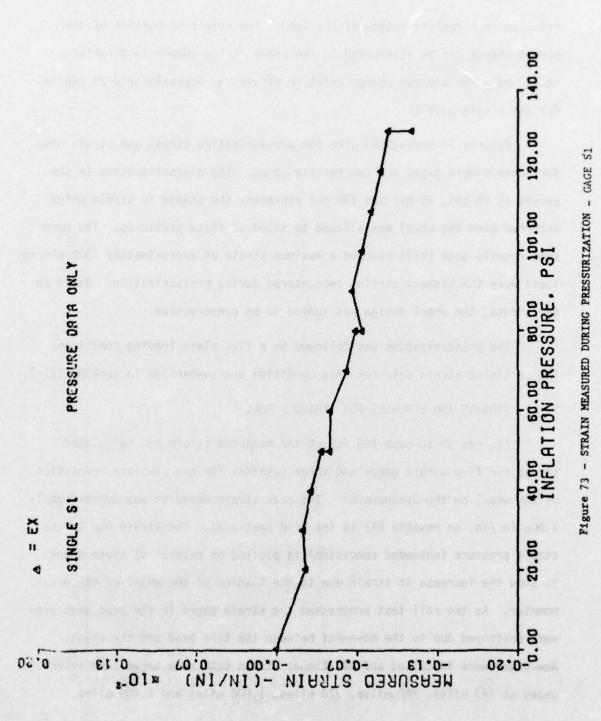
resulted in a redistribution of the load. The remaining portion of the strain change can be attributed to the creep of the composite structure. At 130 psi, the minimum change drift in strain was approximately 20 min/in. for the single gage S1.

Figures 73 through 89 give the pressurization stress and strain data for seven single gages and two rosette gages. The discontinuities in the curves at 50 psi, 80 psi and 130 psi represent the change in strain which occurred when the wheel was allowed to stand at these pressures. The bead seat rosette gage (R12) reached a maximum strain of approximately 1300 min/in. These were the highest strains encountered during pressurization. Based on these data, the wheel design was judged to be conservative.

The pressurization was followed by a flat plate loading condition. The pertinent strain data for this condition are summarized in Section III-2.
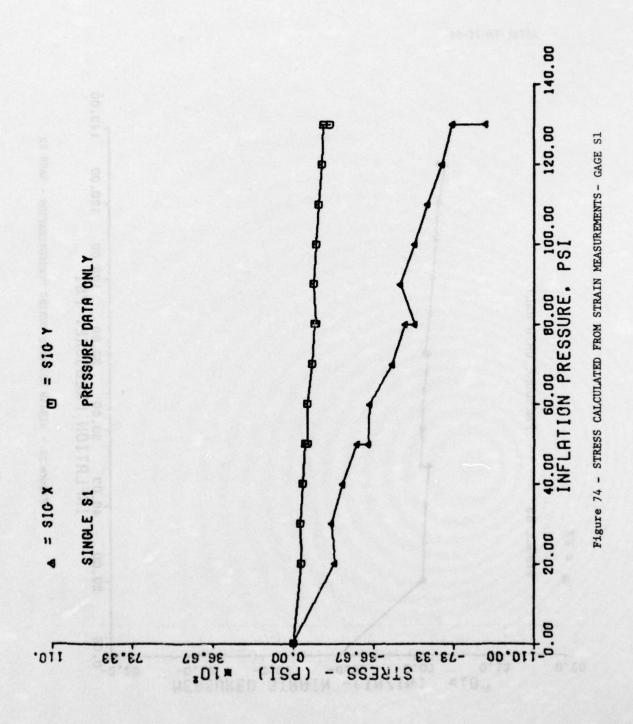
5.   STRAINS AND STRESSES FOR STRAIGHT ROLL

Figures 90 through 105 depict the measured strain and calculated stress for five single gages and three rosettes for one complete revolution of the wheel on the dynamometer. The peak strain measured was approximately 2100μ in./in. on rosette R12 in the bead seat area. The strain due to the static pressure (unloaded condition) is plotted on several of these graphs to show the increase in strain due to the loading of the wheel on the dynamometer. As the roll test progressed the strain gages in the bead seat area were destroyed due to the movement between the tire bead and the wheel. New gages were installed and additional strain data were taken from select gages at 143 miles, 260 miles, 320 miles, 1,000 miles and 1,400 miles.
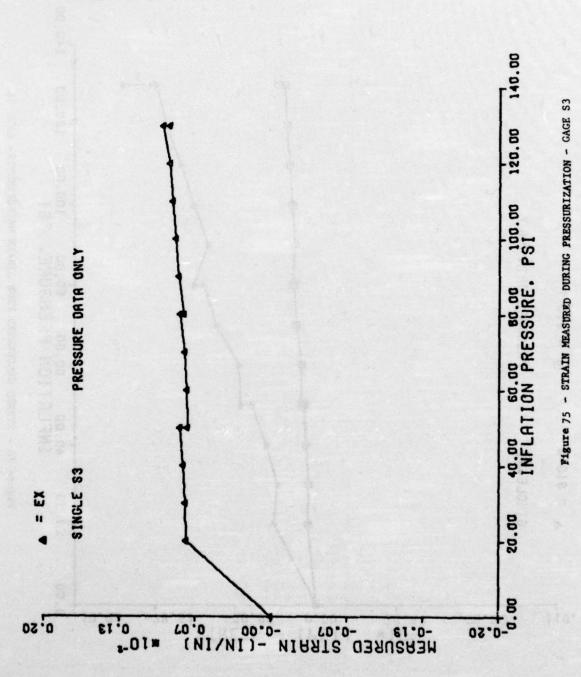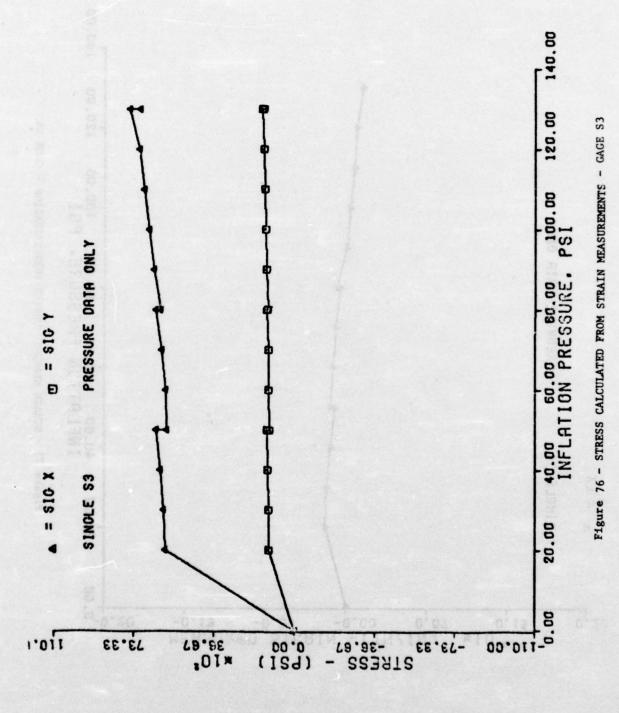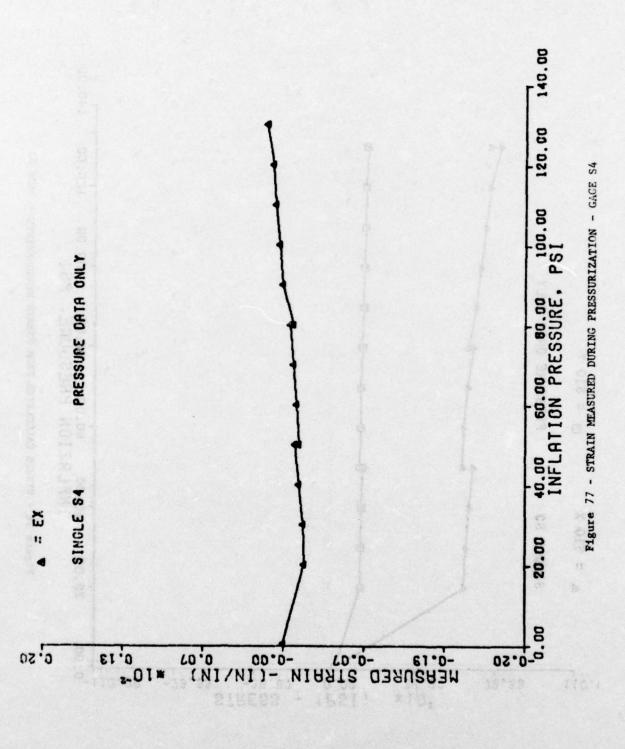
Figure 73 – STRAIN MEASURED DURING PRESSURIZATION – GAGE S1

Figure 74 - STRESS CALCULATED FROM STRAIN MEASUREMENTS - GAGE S1

Figure 75 - STRAIN MEASURED DURING PRESSURIZATION - GAGE S3

106

Figure 76 - STRESS CALCULATED FROM STRAIN MEASUREMENTS - GAGE S3

Figure 77 - STRAIN MEASURED DURING PRESSURIZATION - GAGE S4

Figure 78 – STRESS CALCULATED FROM STRAIN MEASUREMENTS – GAGE S4

Figure 79 - STRAIN MEASURED DURING PRESSURIZATION - GAGE S6

Figure 80 - STRESS CALCULATED FROM STRAIN MEASUREMENTS - GAGE S6

Figure 81 - STRAIN MEASURED DURING PRESSURIZATION - GAGE S8

Figure 82 - STRESS CALCULATED FROM STRAIN MEASUREMENTS - GAGE S8

Figure 83 – STRAIN MEASURED DURING PRESSURIZATION – GAGE S9

Figure 84 - STRESS CALCULATED FROM STRAIN MEASUREMENTS - GAGE S9

Figure 85 - STRAIN MEASURED DURING PRESSURIZATION - GAGE S10

Figure 86 - STRESS CALCULATED FROM STRAIN MEASUREMENTS - GAGE S10

Figure 87 - STRAIN MEASURED DURING PRESSURIZATION - GAGE R8

Figure 88 - STRESS CALCULATED FROM STRAIN MEASUREMENTS - GAGE R8

Figure 89 – STRAIN MEASURED DURING PRESSURIZATION – GAGE R12

Figure 90 - STRESS CALCULATED FROM STRAIN MEASUREMENTS - GAGE R12

Figure 91 - MEASURED STRAIN VS ANGLE OF ROTATION - GAGE S1 STRAIGHT ROLL

AFFDL-TR-76-54

Figure 92 - CALCULATED STRESS VS ANGLE OF ROTATION - GAGE S1 STRAIGHT ROLL

123

Figure 93 – <u>MEASURED STRAIN VS ANGLE OF ROTATION - GAGE S3 STRAIGHT ROLL</u>

▲ = SIG X WHERE ⊡ = SIG Y WHICH DEGREES

SINGLE S3   NUMBER OF MILES = 0
STRAIGHT ROLL

STRESS - (PSI) *10²

ANGLE OF ROTATION, DEGREES

Figure 94 - CALCULATED STRESS VS ANGLE OF ROTATION - GAGE S3 STRAIGHT ROLL

Figure 95 - MEASURED STRAIN VS ANGLE OF ROTATION - GAGE S4 STRAIGHT ROLL

Figure 96 - CALCULATED STRESS VS ANGLE OF ROTATION - GAGE S4 STRAIGHT ROLL

Figure 97 - MEASURED STRAIN VS ANGLE OF ROTATION - GAGE S6 STRAIGHT ROLL

128

Figure 98 - CALCULATED STRESS VS ANGLE OF ROTATION - GAGE S6 STRAIGHT ROLL

Figure 99 – MEASURED STRAIN VS ANGLE OF ROTATION – GAGE S9 STRAIGHT ROLL

Figure 100 - CALCULATED STRESS VS ANGLE OF ROTATION - GAGE S9 STRAIGHT ROLL

Figure 101 - MEASURED STRAIN VS ANGLE OF ROTATION - GAGE R1 STRAIGHT ROLL

Figure 102 - CALCULATED STRESS VS ANGLE OF ROTATION - GAGE R1 STRAIGHT ROLL

Figure 103   MEASURED STRAIN VS ANGLE OF ROTATION - GAGE R8 STRAIGHT ROLL

Figure 104 - CALCULATED STRESS VS ANGLE OF ROTATION - GAGE R8 STRAIGHT ROLL

Figure 105 - MEASURED STRAIN VS ANGLE OF ROTATION - GAGE R12 STRAIGHT ROLL
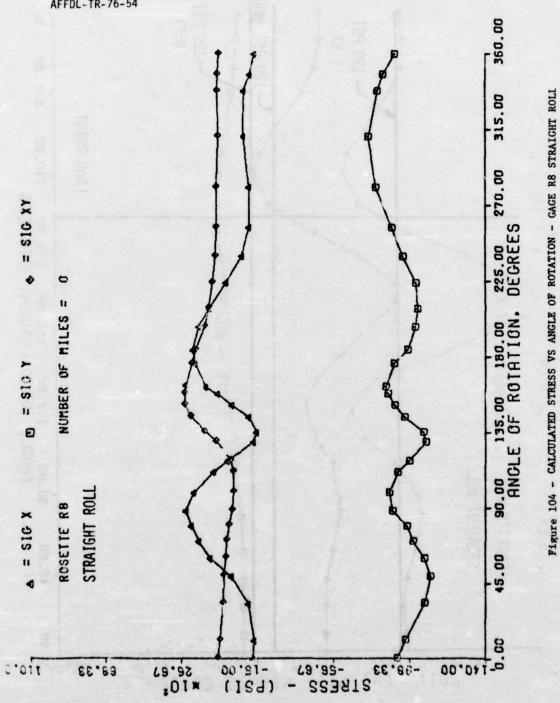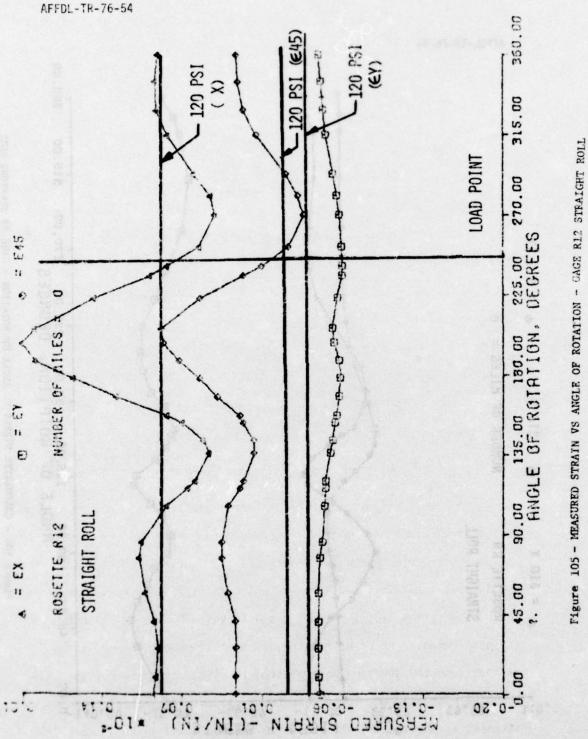
No significant difference was found between the data initially taken and the data taken at a later time. Thus, only the initial data are presented in this report.

6.   STRAINS AND STRESSES FOR CAMBER ROLL

Immediately after collecting the straight roll data, the camber roll data were also taken. These data were very similar to the straight roll data. Figures 106 through 122 depict the strain and stress plots for the same strain gages that were plotted for the straight roll. After the initial data were collected, the wheel was subjected to a 1,400 mile straight slow roll and then 400 miles of cambered slow roll. There were no significant changes in the strain data as a result of completing the straight and camber slow roll, thus only the original data will be shown. As with the straight roll, the maximum strain measured was approximately 2100 µ in./in. on rosette R12 in the bead seat area.
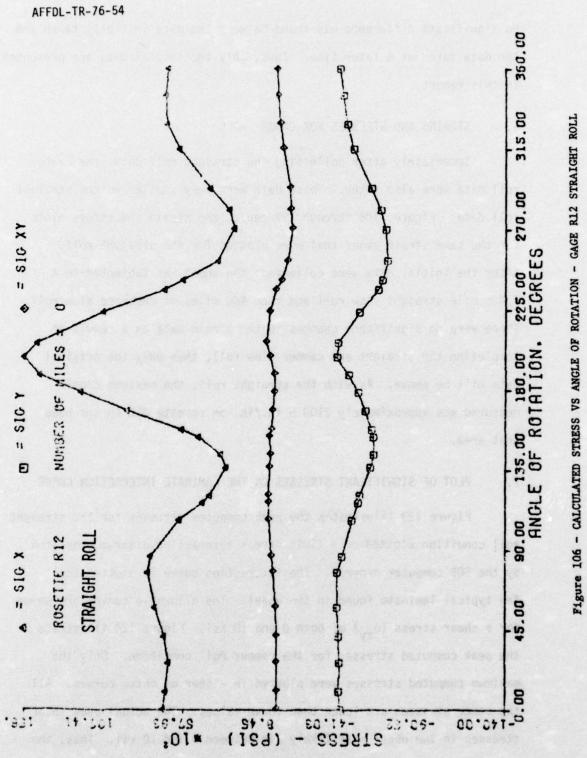
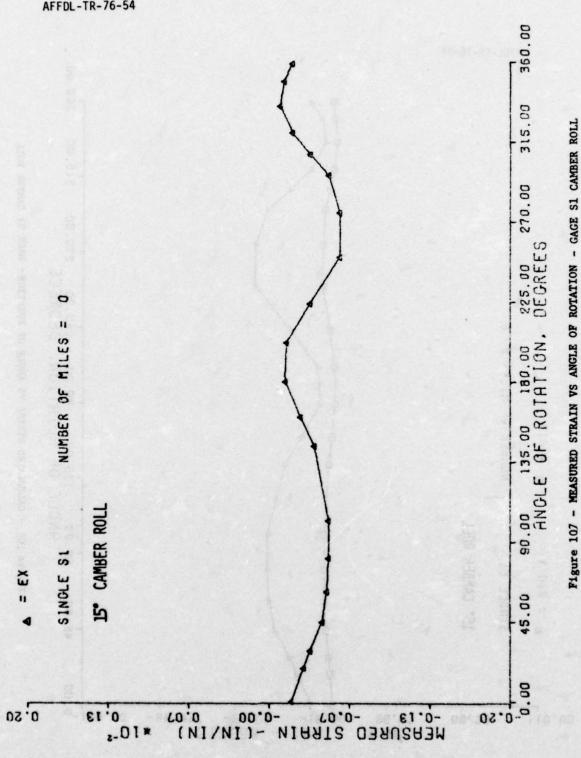7.   PLOT OF SIGNIFICANT STRESSES ON THE LAMINATE INTERACTION CURVE

Figure 123 illustrates the peak computed stresses for the straight roll condition plotted on a limit stress interaction diagram generated by the SQ5 computer program. The interaction curve is plotted for the typical laminate found in the wheel. The allowable curves are shown for a shear stress (σ_{xy}) of both 0 and 10 ksi. Figure 124 illustrates the peak computed stresses for the camber roll condition. Only the maximum computed stresses were plotted in either of these curves. All the other stresses are lower than these values. The actual peak shear stresses in the wheel most likely lie between 0 and 10 ksi. Thus, the
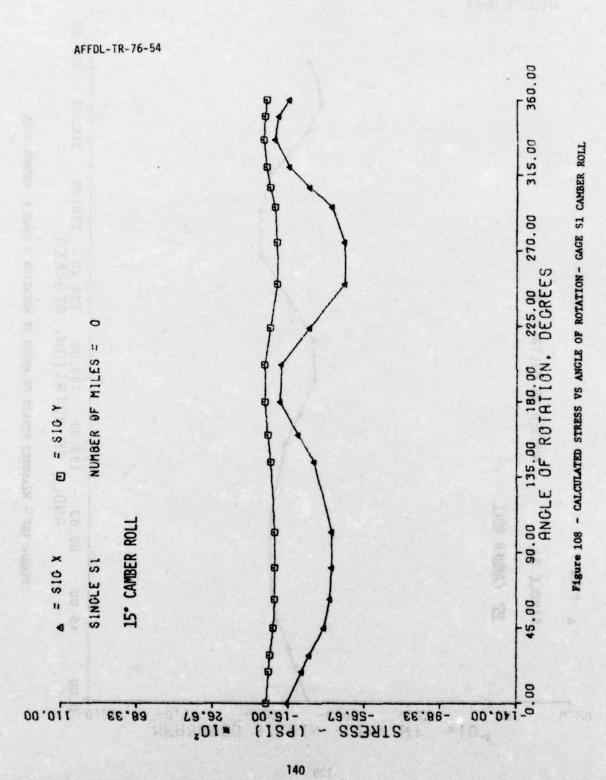
137

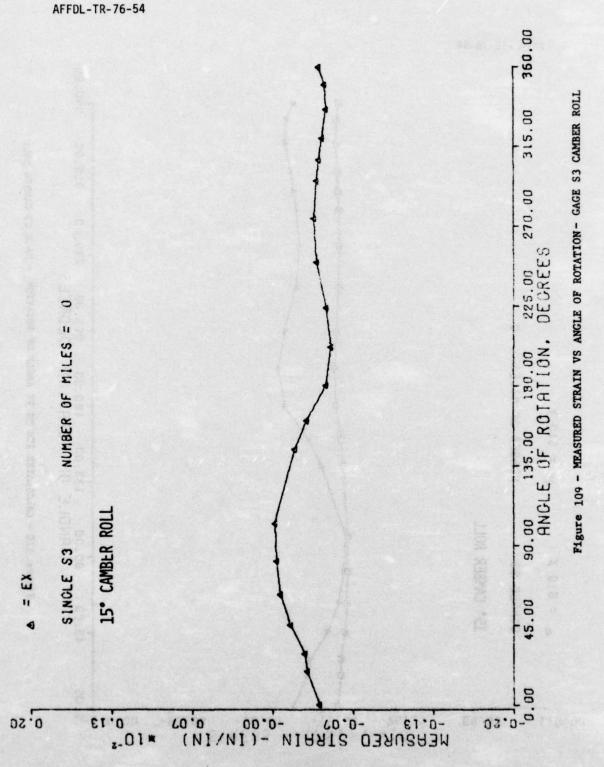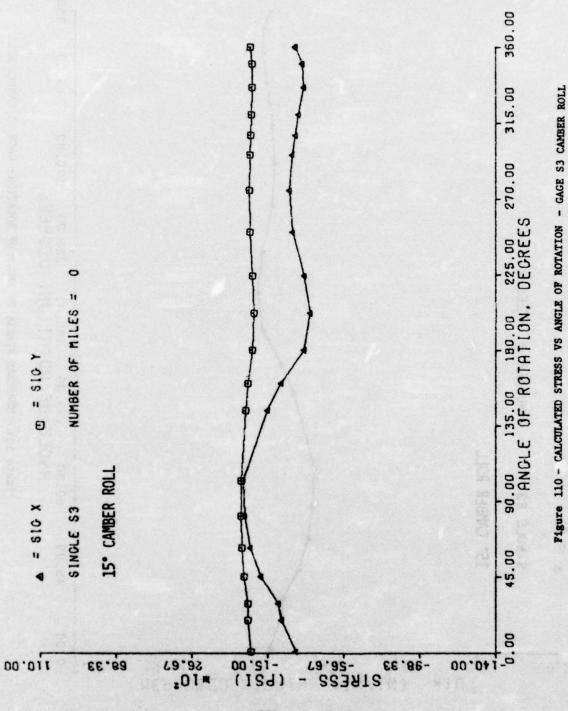Figure 106 - CALCULATED STRESS VS ANGLE OF ROTATION - GAGE R12 STRAIGHT ROLL

Figure 107 - MEASURED STRAIN VS ANGLE OF ROTATION - GAGE S1 CAMBER ROLL

▲ = SIG X   ◇ = SIG Y   □ = SIG Z

SINGLE S1   NUMBER OF MILES = 0

15° CAMBER ROLL

STRESS - (PSI) *10²

110.00   68.33   26.67   -15.00   -56.67   -98.33   -140.00

0.00   45.00   90.00   135.00   180.00   225.00   270.00   315.00   360.00
ANGLE OF ROTATION, DEGREES

Figure 108 - CALCULATED STRESS VS ANGLE OF ROTATION- GAGE S1 CAMBER ROLL

Figure 109 - MEASURED STRAIN VS ANGLE OF ROTATION - GAGE S3 CAMBER ROLL

Figure 110 - CALCULATED STRESS VS ANGLE OF ROTATION - GAGE S3 CAMBER ROLL

Figure 111 - MEASURED STRAIN VS ANGLE OF ROTATION - GAGE S4 CAMBER ROLL

143

AFFDL-TR-76-54

Figure 112 - CALCULATED STRESS VS ANGLE OF ROTATION - GAGE S4 CAMBER ROLL

144

Figure 113 - MEASURED STRAIN VS ANGLE OF ROTATION - GAGE S6 CAMBER ROLL

Figure 114 - CALCULATED STRESS VS ANGLE OF ROTATION - GAGE S6 CAMBER ROLL

Figure 115 - MEASURED STRAIN VS ANGLE OF ROTATION - GAGE S9 CAMBER ROLL

Figure 116 CALCULATED STRESS VS ANGLE OF ROTATION – GAGE S9 CAMBER ROLL

Figure 117 - MEASURED STRAIN VS ANGLE OF ROTATION - GAGE R1 CAMBER ROLL

Figure 118 CALCULATED STRESS VS ANGLE OF ROTATION - GAGE R1 CAMBER ROLL

Figure 119 - MEASURED STRAIN VS ANGLE OF ROTATION - GAGE R8 CAMBER ROLL

Figure 120 - CALCULATED STRESS VS ANGLE OF ROTATION - GAGE R8 CAMBER ROLL

Figure 121 - MEASURED STRAIN VS ANGLE OF ROTATION - GAGE R12 CAMBER ROLL

Figure 122 - CALCUALTED STRESS VS ANGLE OF ROTATION - GAGE R12 CAMBER ROLL

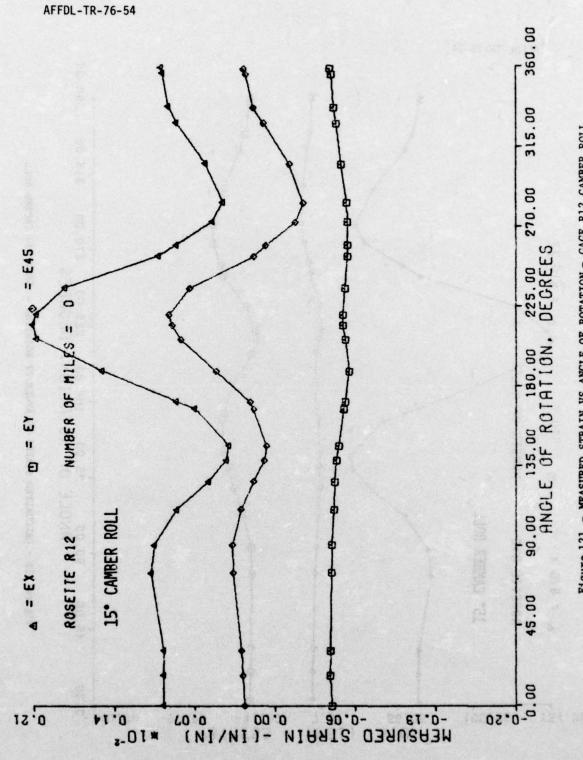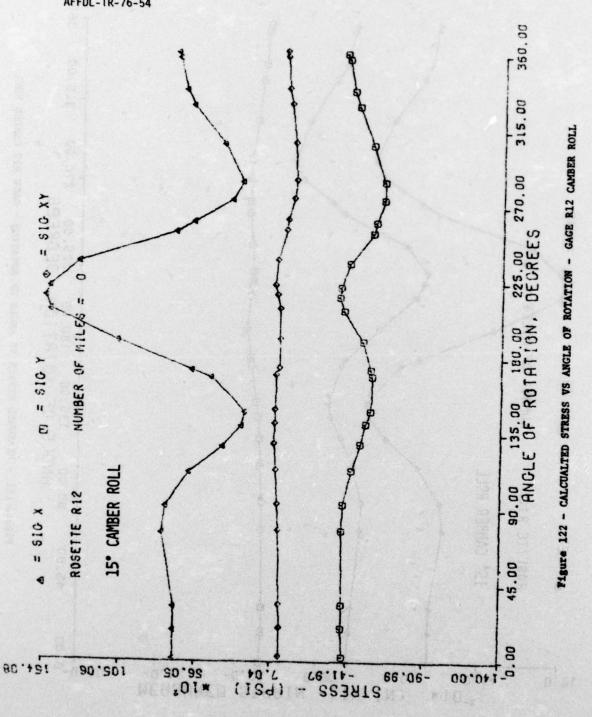Figure 123 — PLOT OF STRAIGHT ROLL STRESSES VS SQ5 LIMIT DESIGN ALLOWABLES

Figure 124 – PLOT OF 15° CAMBER ROLL STRESSES VS SQ5 LIMIT DESIGN ALLOWABLES
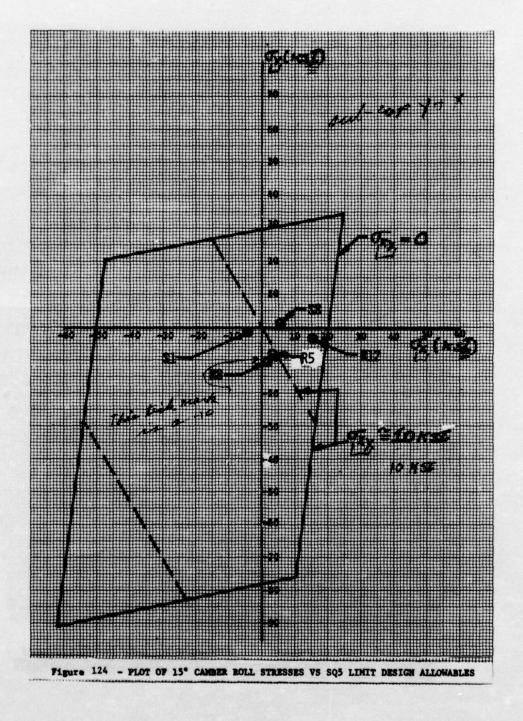
Figure 124 - PLOT OF 15° CAMBER ROLL STRESSES VS SQ5 LIMIT DESIGN ALLOWABLES
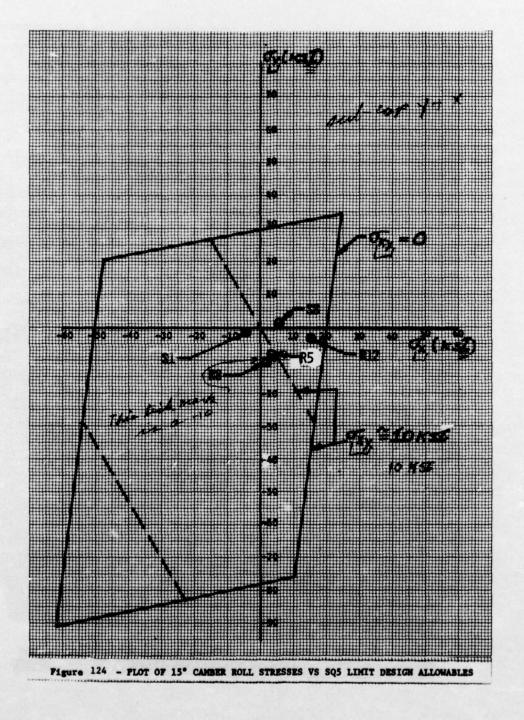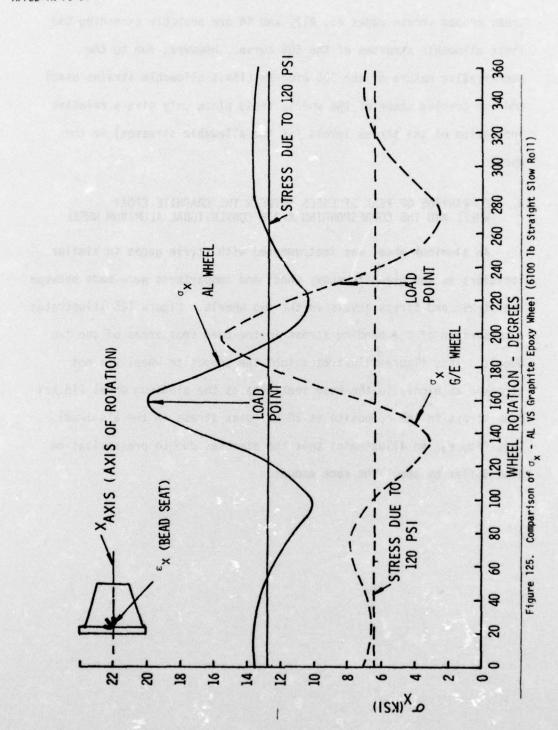
areas around strain gages R5, R12, and S8 are probably exceeding the limit allowable stresses of the SQ5 curve. However, due to the conservative nature of the SQ5 program (limit allowable strains used) and the complex shape of the wheel, these plots only give a relative indication of the stress levels (vs the allowable stresses) in the wheel.

8. COMPARISON OF PEAK STRESSES BETWEEN THE GRAPHITE EPOXY
   WHEEL AND THE CORRESPONDING A-37B CONVENTIONAL ALUMINUM WHEEL

An aluminum wheel was instrumented with strain gages in similar locations as the graphite epoxy wheel and comparisons were made between the strain and stress levels in the two wheels. Figure 125 illustrates a comparison of the bending stress in the bead seat areas of the two wheels. This figure illustrates that the composite wheel was not stressed as highly in the bead seat area as the aluminum wheel (16 ksi peak stress in the composite vs 20 ksi peak stress in the aluminum). This figure also illustrates that the stresses due to pressurization also differ by about the same amount.

Figure 125. Comparison of σ_x – AL VS Graphite Epoxy Wheel (6100 lb Straight Slow Roll)

SECTION V

CONCLUSIONS

This test has demonstrated the feasibility and durability of an unbraked graphite epoxy aircraft wheel. Although the wheel may appear to be fragile, in reality it is extremely tough and durable. Also, even though the wheel was not highly stressed (as shown by the computed stresses), a weight savings of 16 percent was obtained over the comparable metal wheel. The wheel had excellent fatigue life as demonstrated by the large number of roll miles attained before fatigue cracks developed. When the wheel did fail, it was not a catastrophic failure, as might be expected in a metal wheel, but instead it was just a gradual loss of air. The safety ramifications of this failure are a possible technical breakthrough.

SECTION VI

RECOMMENDATIONS

(1) Reduce the Fabrication Costs

The wheel was a very expensive item to make because of the vast amount of hand labor required during the lay-up of the plies. The fabrication method needs to be simplified and automated to reduce these costs.

(2) Develop Relaxed Manufacturing Tolerances

Tests need to be conducted to determine the amount of variance allowed during the manufacturing process.

(3) Test Additional Wheels

Repeat these tests for at least three more wheels of similar design.

(4) Additional Efforts

Apply this technology to high temperature composites so that a wheel could be developed to be compatible with an aircraft brake.

(5) NDI

Additional methods of nondestructive inspection should be developed. Also, some methods must be developed to quantify what is observed in the NDI and relate this to wheel strength.

(6) Environmental Effects Tests

Tests should be conducted to determine the effects of moisture on the structural integrity of the composite.

REFERENCES

1. AF Dwg 67J1951, <u>Wheel-Brake and Tire Assembly - Main Gear - Size 7.00-8</u>, 13 February 1967.

2. A. L. Price, <u>Filament Composite Wheel Development for Military Aircraft</u>, AFFDL-TR-71-144, October 1971.

3. J. E. Ashton, J. C. Halpin, P. H. Petit, <u>Primer on Composite Materials & Analysis</u>, Technomic Publishing Co., 1969.

4. Stephan W. Tsai, <u>Mechanics of Composite Materials</u>, AFML-TR-66-149, Part I and Part II, June 1966.

5. <u>Structural Design Guide for Advanced Composite Applications</u>, Third Edition, Los Angeles Division of the North American Rockwell Corp., AFML Contract F33615-69-C-1368, January 1973.

6. Dr. D. L. Reed, <u>Point Stress Laminate Analysis</u>, General Dynamics (Fort Worth) document FZM-5494, AF Contract F33615-69-C-1494, 1 April 1970.